

Multidimensional trait space informed by a mechanistic model of tree growth and carbon allocation

MICHAEL FELL,^{1,2,†} JARRETT BARBER,² JEREMY W. LICHSTEIN,³ AND KIONA OGLE^{2,4,5}

¹*School of Life Sciences, Arizona State University, P.O. Box 874501, Tempe, Arizona 85287 USA*

²*School of Informatics, Computing, and Cyber Systems, Northern Arizona University, P.O. Box 5693, Flagstaff, Arizona 86011 USA*

³*Department of Biology, University of Florida, P.O. Box 118525, Gainesville, Florida 32611 USA*

⁴*Center for Ecosystem Science and Society, Northern Arizona University, P.O. Box 5620, Flagstaff, Arizona 86011 USA*

⁵*Department of Biological Sciences, Northern Arizona University, P.O. Box 5640, Flagstaff, Arizona 86011 USA*

Citation: Fell, M., J. Barber, J. W. Lichstein, and K. Ogle. 2018. Multidimensional trait space informed by a mechanistic model of tree growth and carbon allocation. *Ecosphere* 9(1):e02060. 10.1002/ecs2.2060

Abstract. Plant functional traits research has revealed many interesting and important patterns among morphological, physiological, and life-history traits and the environment. These are exemplified in trade-offs between groups of traits such as those embodied in the leaf and wood economics spectra. Inferences from empirical studies are often constrained by the correlative nature of the analyses, availability of trait data, and a focus on easily measured traits. However, empirical studies have been fundamental to modeling endeavors aiming to enhance our understanding of how functional traits scale up to affect, for example, community dynamics and ecosystem productivity. Here, we take a complementary approach utilizing an individual-based model of tree growth and mortality (the allometrically constrained growth and carbon allocation [ACGCA] model) to investigate the theoretical trait space (TTS) of North American trees. The model includes 32 parameters representing allometric, physiological, and anatomical traits, some overlapping leaf and wood economics spectra traits. Using a Bayesian approach, we fit the ACGCA model to individual tree heights and diameters from the USFS Forest Inventory and Analysis (FIA) dataset, with further constraints by literature-based priors. Fitting the model to 1.3 million FIA records—aggregated across individuals, species, and sites—produced a posterior distribution of traits leading to realistic growth. We explored this multidimensional posterior distribution (the TTS) to evaluate trait–trait relationships emerging from the ACGCA model, and compare these against empirical patterns reported in the literature. Only three notable bivariate correlations, among 496 possible trait pairs, were contained in the TTS. However, stepwise regressions uncovered a complicated structure; only a subset of traits—related to photosynthesis (e.g., radiation-use efficiency and maintenance respiration)—exhibited strong multivariate trade-offs with each other, while half of the traits—mostly related to allometries and construction costs—varied independently of other traits. Interestingly, specific leaf area was related to several rarely measured root traits. The trade-offs contained in the TTS generally reflect mass-balance (related to carbon allocation) and engineering (mostly related to allometries) trade-offs represented in the ACGCA model and point to potentially important traits that are under-explored in field studies (e.g., root traits and branch senescence rates).

Key words: forest inventory and analysis (FIA); individual-based model; Markov chain Monte Carlo; North American trees; plant functional traits; trait space; trait trade-offs; tree growth model.

Received 20 October 2017; accepted 23 October 2017. Corresponding Editor: Debra P. C. Peters.

Copyright: © 2018 Fell et al. This is an open access article under the terms of the Creative Commons Attribution License, which permits use, distribution and reproduction in any medium, provided the original work is properly cited.

† **E-mail:** michael.fell@nau.edu

INTRODUCTION

Plant functional traits research has led to the discovery of important patterns among morphological, physiological, and life-history traits and between such traits and the environment. In trees, key functional traits include properties of leaves/needles, wood/stems, and roots that are important determinants of plant functions, such as water transport, carbon gain, mechanical limitations, and nutrient uptake (Wright et al. 2004, Chave et al. 2009, Reich 2014). Many trait trade-offs or correlations (e.g., leaf lifespan increases with leaf mass per area; relative growth rate decreases with wood density) have been uncovered through empirical studies, based on trait measurements of hundreds (Reich et al. 1997, Baraloto et al. 2010) to thousands (Wright et al. 2004, Shipley et al. 2006, Chave et al. 2009) of species. Using a variety of regression and ordination techniques, these studies have successfully shown how functional trait relationships relate to theoretical expectations. However, the statistical models (mostly correlational methods) underlying such empirical studies do not directly include a representation of the underlying mechanisms predicted by theory. Thus, there is an opportunity to enhance our understanding of the trait space occupied by trees through the use of mechanistic models that explicitly include, for example, engineering and mass-balance relationships (e.g., Scheiter et al. 2013), in addition to important environmental drivers.

Integration of functional traits with mechanistic models has been a focus of recent research aimed at improving parameterization of dynamic global vegetation models (DGVMs; Scheiter et al. 2013, Fyllas et al. 2014, Sakschewski et al. 2015). Trait-based mechanistic models of patch- and landscape-scale vegetation dynamics have also been used to explore the sensitivity of net primary productivity to different plant traits (Falster et al. 2011), and how trait trade-offs and disturbance can lead to diverse communities with many coexisting species (Falster et al. 2017). Other trait-based modeling studies have utilized trade-offs between functional traits to better understand community-level trait patterns, with the goal of improving predictions of how vegetation and climate interact to influence primary

productivity (Scheiter et al. 2013), or to evaluate how trait distributions vary across large regions (Sakschewski et al. 2015). In general, these types of studies share a common goal of understanding how functional traits influence plant, ecosystem, community, and/or global properties of interest, but they generally do not use the mechanistic model to infer functional traits and potential trade-offs between traits.

The aforementioned empirical or correlative approaches to understanding trait relationships have been instrumental to understanding where organisms lie within a trait spectrum (e.g., trait trade-offs or life-history dimensions). For instance, the leaf economics spectrum (LES) quantifies trade-offs among leaf mass per area (LMA), leaf lifespan (LL), mass-normalized photosynthetic capacity (A_{mass}), leaf nitrogen (N_{mass}), leaf phosphorus (P_{mass}), and leaf dark respiration (R_{mass} ; Wright et al. 2004). Trait–environment relationships are also often evaluated; for instance, LES traits are often correlated with mean annual rainfall and temperature (Wright et al. 2004). Another spectrum relevant to trees is the wood economics spectrum (WES), which links wood traits to major ecological functions, including competitive ability, resistance to stress, and disturbance responses (Chave et al. 2009). An important trade-off revealed by the WES is that growth and mortality rates are both negatively correlated with wood density (Chave et al. 2008, 2009). A third proposed spectrum, the worldwide “fast–slow” economics spectrum, integrates key leaf, wood, and fine root traits, including those in the LES and WES, into a single spectrum by demonstrating consistent trade-offs between traits leading to fast vs. slow growth (Reich 2014). Although the validity and interpretation of some trait spectra have been questioned (Lloyd et al. 2013, Osnas et al. 2013), there is still broad interest in quantifying empirical trait spectra (Díaz et al. 2016) and using these patterns to improve representation of plant functional diversity in models such as DGVMs (Scheiter et al. 2013, Van Bodegom et al. 2014, Fisher et al. 2015). Yet, the underlying factors giving rise to empirical patterns are not always clear and likely emerge from different types of trade-offs, such as those related to resource allocation or physical constraints (Scheiter et al. 2013).

Standard approaches to inferring trait spectra or trade-offs from direct measurements of functional traits include various types of regression analyses (Reich et al. 1999, Wright et al. 2004, Adler et al. 2014, Atkin et al. 2015) and ordination methods (Reich et al. 1999, Cavender-Bares et al. 2004, Díaz et al. 2004, Baraloto et al. 2010, Stahl et al. 2013). Often, the goal of such analyses is to discover how functional traits relate to other traits, to an emergent process (e.g., rates of survival, growth, reproduction), to the environment, or to reduce the dimensionality of the potential trait space by identifying key trade-offs. We refer to these common approaches (i.e., regression and ordination methods) as describing “empirical trait spectra” because they are revealed by direct analyses of trait data collected on plants, often growing in field conditions. These studies provide vital insights, but may be limited by the traits they assess, favoring traits that are easy to measure over those that are more difficult to quantify (Weiher et al. 1999, Lavorel and Garnier 2002, Lavorel et al. 2007). It is likely, however, that such under-represented traits are important for predicting whole-plant function. These potential limitations may render empirical spectra inappropriate for predicting plant function under novel conditions (Webb et al. 2010, Evans 2012, Scheiter et al. 2013).

To move beyond empirical or phenomenological models of trait relationships, and to develop the capacity to predict plant function under future or novel environments, trade-offs should be related to plant function and underlying processes and mechanisms. Scheiter et al. (2013) envisaged that trait trade-offs fall into one of three categories describing mechanisms that give rise to the trade-offs, and they suggested that this could facilitate incorporating a trait perspective into DGVMs. These include (1) mass conservation trade-offs related to resource use and allocation, (2) engineering trade-offs that prevent structures or architectures of plants that are not feasible, and (3) empirical trade-offs that are more difficult to derive mathematically and that are not explicitly considered in a given modeling framework (Scheiter et al. 2013). We propose a complimentary approach to understanding trait spectra that takes these considerations into account by using a trait-based, process model of whole-plant function to determine how

functional traits interact with each other to influence whole-plant function (e.g., growth and survival).

Thus, to produce realistic behavior of whole-plant performance, mechanistic models should consider important mass-balance processes—such as those related to plant physiological processes (e.g., photosynthesis, respiration) and carbon allocation (mass conservation trade-offs)—and engineering constraints—such as structural characteristics (e.g., anatomical features), and allometric relationships. Examples include the many existing individual-based models (IBMs) of plant growth (Bugmann 2001, Ogle and Pacala 2009, Fyllas et al. 2014). Such models are useful in relating key traits—which usually take the form of model parameters—to processes such as carbon acquisition, allocation, and metabolism and provide a novel way of investigating the influence of key functional traits (model parameters) on growth and/or survival (model outputs). By fitting IBMs to empirical data on plant performance and functional traits, it may be possible to investigate the “theoretical trait space” that emerges from the mass conservation and engineering trade-offs (Scheiter et al. 2013) that are built into the IBM. Evaluation of the theoretical trait space (or spectra) should provide insight into how plant performance and/or trade-offs relate to the range of traits observed. Using mechanistic models to estimate trait values also provides an opportunity to better understand how under-represented (rarely measured) traits may influence tree growth and/or survival.

The main objectives of this study were to (1) quantify the theoretical trait space (TTS) of North American trees, (2) evaluate the TTS to determine which traits are important predictors of tree growth and which trade off with each other to influence growth, and (3) use this TTS to better understand how patterns in empirical trait spectra (e.g., LES and WES) arise. To accomplish these objectives, we fit an IBM of tree growth and survival, the allometrically constrained growth and carbon allocation (ACGCA) model (Ogle and Pacala 2009), to 1.27 million growth observations of “healthy” trees from the USFS Forest Inventory and Analysis (FIA) database that were pooled across sites, species, and individuals, complemented by literature information (TreeTraits database; Kattge et al. 2011, Ogle

et al. 2013, 2014) to help constrain parameter values (traits) to realistic ranges. To achieve this, we employed a Bayesian framework that utilized a fast, custom stochastic algorithm for fitting the ACGCA model to the aggregated FIA data and literature information, which produced a 32-dimensional (joint) posterior distribution of parameters (traits) that lead to realistic tree growth. We refer to this joint posterior as the TTS, and we evaluated the TTS to address the following questions: (1) Do bivariate or higher dimensional relationships exist between traits in the TTS, and if so, which traits contribute to these relationships? (2) Which traits are the best predictors of growth and what is the role that these traits play in the TTS? (3) How does the TTS compare to empirical spectra such as the LES and WES?

METHODS

Overview

We fit the ACGCA model (Ogle and Pacala 2009) to USFS Forest Inventory and Analysis (FIA) data on individual tree heights and stem diameters within a Bayesian framework to investigate the TTS of North American trees. Computational challenges involved with fitting the ACGCA model to the large FIA dataset and the limitations of precompiled software—such as JAGS (Plummer 2003) or OpenBUGS (Lunn et al. 2009) for conducting Bayesian analysis—necessitated development of a customized Metropolis-Hastings (MH) algorithm. In addition to fitting the ACGCA model to the FIA data, model parameters (Table 1) were partially constrained by priors derived from the TreeTraits database (Kattge et al. 2011, Ogle et al. 2013, 2014). Below, we first summarize the ACGCA model; then, we provide an overview of the data sources used to inform the ACGCA model, followed by a description of the Bayesian approach used to fit the ACGCA model to the data, including a description of the custom MH algorithm and how the Bayesian results were analyzed.

Tree growth and carbon allocation model

The ACGCA model is an IBM of tree growth and mortality (Ogle and Pacala 2009). The ACGCA model recognizes the importance of including both allometric relationships (related

to engineering trade-offs) and physiological (mass balance) processes underlying labile and structural carbon dynamics, including allocation and growth (Ogle and Pacala 2009); these processes are governed by 32 functional traits (i.e., model parameters; see Table 1). Tree growth is simulated by dynamically allocating labile carbon to storage and structural biomass pools in a way that obeys observed allometric relationships among leaf, stem, branch, and root compartments (Ogle and Pacala 2009). Structural (biomass) pools of different tissue compartments (leaves; fine roots; and root, branch, and trunk sapwood and heartwood) are predicted at each time step.

Labile carbon dynamics are essential to the ACGCA model. There are two main types of labile carbon storage pools. One is associated with storage in leaf and fine root tissue, and labile carbon in this pool is retranslocated when structural tissue is lost (e.g., via senescence of leaves or fine roots). The other storage pool is associated with storage in sapwood and can be drawn upon during times of stress (high labile carbon demand). The ACGCA model also includes a transient labile carbon pool (e.g., recent photosynthesis and retranslocated carbon) that is not associated with storage in any specific tissue and is immediately redistributed within the plant to accommodate structural biomass production, growth respiration, and allocation to storage pools (Ogle and Pacala 2009).

Labile carbon allocation and storage aligns with six physiological states: healthy, static, shrinking, recovering, recovered, or dead. Each physiological state is described by a set of difference equations that satisfy mass-balance relationships among the structural and labile carbon pools (Eqs. 4–8, below). Negative carbon balance (demand > supply) results in a “reduced” allometry, an unhealthy state, and eventual tree death. To quantify the TTS of living trees, we only focus on the healthy state because we are interested in understanding the traits that underlie tree growth, of living trees; in a subsequent study, we also explore the trait space of trees that succumb to environmental stress (M. Fell and K. Ogle, *unpublished manuscript*). In the healthy state, labile carbon is allocated so that the sizes of the structural and storage pools are kept in allometric proportion by solving a set of difference

Table 1. Descriptions and units associated with the 32 parameters (θ_q 's) in the ACGCA model that are representative of potentially important functional traits.

Symbol	Unit	Description
H_{max}	m	Maximum tree height
φ_H	–	Slope at H vs. r curve at $r = 0$ m
η	–	Relative height at which trunk transitions from paraboloid to cone
SW_{max}	m	Maximum sapwood width
λ_S	–	Proportionality between B_T and B_O for sapwood
λ_H	–	Proportionality between B_T and B_O for heartwood
ρ	g dw/m ³	Wood density
f_1	–	Fine root area-to-leaf area ratio
f_2	–	Leaf area-to-xylem conducting area ratio
γ_C	g gluc/m ³	Maximum storage capacity of living sapwood cells
γ_w	m ³ g/dw	(Inverse) density of sapwood structural tissue
γ_X	–	Xylem conducting area-to-sapwood area ratio
C_{GL}	g gluc g/dw	Construction costs of producing leaves
C_{GR}	g gluc g/dw	Construction costs of producing fine roots
C_{GW}	g gluc g/dw	Construction costs of producing sapwood
δ_L	g gluc g/dw	Labile carbon storage capacity of leaves
δ_R	g gluc g/dw	Labile carbon storage capacity of fine roots
S_L	year ⁻¹	Senescence rate of leaves
SLA	m ² g/dw	Specific leaf area
S_R	year ⁻¹	Senescence rate of fine roots
S_O	year ⁻¹	Senescence rate of coarse roots and branches
r_R	m	Average fine root radius
ρ_R	g dw/m ³	Tissue density of fine roots
R_{mL}	g gluc g·dw ⁻¹ ·year ⁻¹	Maintenance respiration rate of leaves
R_{mS}	g gluc g·dw ⁻¹ ·year ⁻¹	Maintenance respiration rate of sapwood
R_{mR}	g gluc g·dw ⁻¹ ·year ⁻¹	Maintenance respiration rate of fine roots
η_B	–	Relative height at which trunk transitions from neiloid to paraboloid
k	–	Crown light extinction coefficient
ε	g gluc/MJ	Radiation-use efficiency
m	–	Maximum relative crown depth
α	–	Crown curvature parameter
R_0	m	Maximum potential crown radius of a tree with diameter at breast height of 0 m (i.e., for a tree that is exactly 1.37 m tall)
R_{40}	m	Maximum potential crown radius of a tree with diameter at breast height of 0.4 m (40 cm)

equations that tie the size of each pool to trunk radius. Below, we highlight key aspects of the ACGCA model relevant to this study and note specific functional traits relevant to these processes; a full description of the model is given in Ogle and Pacala (2009).

Light is the only environmental driving variable in the current version of the ACGCA model. A simple radiation-use function is applied to determine the amount of labile carbon fixed by a tree (gross photosynthesis, P_G) per year:

$$P_G(t) = \varepsilon \cdot APAR(t) \quad (1)$$

where ε is radiation-use efficiency (a functional trait), $APAR$ is the absorbed photosynthetically

active radiation (PAR), and t is time (years). Absorbed photosynthetically active radiation is based on the maximum annual PAR above the tree's crown (PAR_{max}), modified by the light extinction coefficient of the tree's crown (k , a trait), its leaf area (LA), and its leaf area index (LAI) using the Beer-Lambert equation (Ogle and Pacala 2009):

$$APAR(t) = PAR_{max} \left\{ 1 - \exp(-k \cdot LAI(t - \Delta t)) \right\} \cdot \left(\frac{LA(t - \Delta t)}{LAI(t - \Delta t)} \right) \quad (2)$$

The numerical time step, Δt , is set to 1/16 of a year to achieve numerical convergence, and the

model outputs individual tree states at an annual timescale (Ogle and Pacala 2009). The effect of light was tested by running simulations that varied PAR_{max} from 10% (e.g., representing an overtopped tree in a dense canopy) to 100% (an open-grown tree) of the maximum incident radiation expected above the forest canopy, following a logarithmic progression (206, 259, 326, 411, 517, 651, 820, 1032, 1300, 1636, 2060 MJ·m⁻²·yr⁻¹), yielding 11 light levels. Leaf area is assumed to be related to xylem conducting area (XA , a trait) via an allometric function. Leaf area index is equal to LA divided by the tree's projected crown area (Ogle and Pacala 2009).

The amount of "excess" labile carbon, $E(t)$, determines the size of the transient pool available for biomass production at time t . $E(t)$ is computed as a simple mass balance that first scales up area-specific photosynthesis to tree-level carbon assimilation (input variable) as $P_G(t) \cdot LA(t - \Delta t)$. Other inputs to $E(t)$ are associated with retranslocation of labile carbon from senescing leaf and root tissues and sapwood-to-heartwood conversion (incorporated through δ terms explained below). Losses from $E(t)$ are attributed to maintenance respiration (R_M) of all living tissues (tissue-specific trait). Thus, $E(t)$ is given by:

$$E(t) = P_G(t) \cdot LA(t - \Delta t) + \delta_S(t) \cdot S_O \cdot B_{OS}(t - \Delta t) + \sum_{i=L,R} \delta_i \cdot S_i \cdot B_i(t - \Delta t) - R_M(t) \quad (3)$$

Key traits (parameters) here include δ_S , δ_L and δ_R (g gluc g/dw), which are the labile carbon storage capacities of sapwood, leaves, and fine roots, respectively (see Ogle and Pacala 2009 for full derivation of δ terms). B_{OS} , B_L and B_R (g dw) are state variables that represent the structural biomass of other (e.g., branches and coarse roots) sapwood, leaves, and fine roots, and S_O , S_L and S_R are their corresponding senescence rates (also traits/parameters; Ogle and Pacala 2009).

Excess labile carbon (when $E > 0$) is subsequently allocated to the different tissue compartments to produce structural biomass, B_i , where $i = L$ (leaves), R (fine roots), TS (trunk sapwood), TH (trunk heartwood), OS (other sapwood, i.e., sapwood of branches and coarse roots), and OH (other heartwood). For each time step in the model, the excess carbon allocated to each

compartment is simultaneously converted to biomass and allocated to storage according to each tissue's labile carbon storage capacity (δ 's, as defined above). The allocation of labile carbon and production of structural carbon must satisfy constraints set by the tree's allometric relationships, which are tied to the radius (r) of the tree's trunk such that for a tree growing according to the healthy allometry (Ogle and Pacala 2009):

$$\Delta B_{OS} = \lambda \cdot \Delta B_{TS} \quad (4)$$

$$\Delta B_{OH} = \lambda \cdot \Delta B_{TH} \quad (5)$$

$$\frac{\Delta LA(r(t))}{SLA} = \Delta B_L \quad (6)$$

$$\rho_R \cdot \frac{r_R}{2} \cdot \Delta RA(r(t)) = \Delta B_R \quad (7)$$

$$\rho(t) \cdot \Delta V_T(r(t)) = \Delta B_T \quad (8)$$

The ΔB_i 's denote the change in structural biomass in a given time step. Allometric relationships are incorporated via the changes in LA (ΔLA), fine root area (ΔRA), and trunk volume (ΔV_T), which are expressed as functions of trunk radius at time t , $r(t)$, as per the healthy allometry. The traits (parameters) λ , specific leaf area (SLA), r_R , ρ_R , and ρ (see Table 1 for definitions) link the allometric and mass-balance constraints.

Eqs. 4–8 are solved numerically using a root-finding routine (Ogle and Pacala 2009), yielding solutions for r and all other state variables (e.g., LA , RA , B 's), including tree height (H), which is linked to r by a simple allometric equation:

$$H(t) = H_{max} \cdot \left\{ 1 - \exp\left(-\frac{\varphi_H}{H_{max}} \cdot r(t)\right) \right\} \quad (9)$$

Two key allometric traits are the maximum tree height, H_{max} , and the initial (at $r = 0$) slope of the H vs. r allometric curve, φ_H .

For the purpose of fitting the ACGCA model to FIA data, the model can be viewed as a nonlinear function of the vector of parameters (traits) and inputs (e.g., light or PAR_{max} ; Table 1) that yields outputs such as H and r for each year of the simulation.

Data sources

The ACGCA model parameters are informed by two primary data sources: the FIA data compiled by the U.S. Forest Service (<http://www.fia.fs.fed.us/>) and the TreeTraits database compiled from published literature (Kattge et al. 2011, Ogle et al. 2013, 2014; see *Tree functional traits database*). The FIA database provided repeated measurements for radius and height data for 965,003 individual trees occurring in approximately 100,779 plots that are an unbiased sample of forested areas in the United States (Bechtold and Patterson 2005).

Forest inventory data

The FIA data were filtered such that only living individuals with at least two height and diameter measurements were included in the study to facilitate calculating changes in radius (Δr) and height (ΔH). The data were further filtered to select for “healthy,” growing trees such that an individual was discarded if (1) it was missing r and/or H values, (2) $\Delta r \leq 0$ or $\Delta H \leq 0$, (3) $r < 0.05$ m (the starting radius for the ACGCA simulations), or (4) the annualized Δr or ΔH values were larger than the 99.9% quantile of all data (i.e., remove outliers). The resulting, filtered FIA dataset (1,270,510 remeasurements) had minimum and maximum (min, max) r , H , Δr , and ΔH values of (0.050 m, 0.923 m), (0.051 m, 78.030 m), (3.24×10^{-5} m/yr, 0.012 m/yr), and (1.23×10^{-2} m/yr, 3.360 m/yr), respectively.

The sheer size of the FIA data precludes fitting the ACGCA model to individual- or tree-level data as this would greatly exceed available computational resources. Thus, to quantify the distribution of observed tree growth based on the FIA data, the r , H , Δr , and ΔH data were log-transformed and used to construct a four-dimensional histogram describing the distribution of “realistic” values corresponding to healthy, growing trees. The histogram had nine evenly spaced bins in each dimension ($9^4 = 6516$ total bins). The number of bins was chosen based on trial and error to provide sufficient resolution for analysis, but avoiding excessive computational issues associated with using more bins. Limits in each dimension were based on the minimum and maximum values in the filtered FIA data, with the exception of the minimum value for r , which was set to 0.05. Each point (r_i , H_i , Δr_i , ΔH_i) representing an individual tree with multiple

measurements was assigned to a bin, for $i = 1, 2, \dots, 1,270,510$ remeasurement points. The proportion of trees falling in each of the 6561 bins was computed, yielding a four-dimensional probability distribution (or histogram) of the FIA data (henceforth referred to as *Hist*), aggregated across individuals, species, and sites.

Tree functional traits database.—Data from the TreeTraits database (Kattge et al. 2011, Ogle et al. 2013, 2014) were used to derive semi-informative priors to constrain the parameters (traits) to realistic ranges. TreeTraits contains summary statistics (e.g., sample means or parameter estimates) for functional traits extracted from the literature for the ca. 300 tree species represented in the FIA database. TreeTraits provided over 7400 records for 27 functional traits, with sample sizes ranging from 6 (r_r and ρ_r) to >1700 (*SLA* and ρ ; see Table 1 for parameter/trait descriptions). The Bayesian model (see *Bayesian model*) requires priors for log- or logit-scale parameters, and means and standard deviations of the transformed values (log or logit; Appendix S1: Table S1) were derived from the TreeTraits database and used to construct semi-informative priors. The TreeTraits database lacked data for λ_{sr} , λ_{lv} , f_L , η_B , and m (see Table 1 for definitions); in these cases, the prior means were set to the values used for *Pinus taeda* and *Acer rubrum* in Ogle and Pacala (2009), and the prior standard deviations were set to constrain parameters to magnitudes similar to *A. rubrum* and *P. taeda* in Ogle and Pacala (2009). See Appendix S1: Table S1 for the prior distributions.

Bayesian model

The ACGCA model was fit to the FIA data in a Bayesian framework to yield posterior distributions of parameters (traits) leading to “realistic” tree growth based on the FIA data and partially constrained by the priors. The basic Bayesian formulation defines the posterior distribution of the parameters, conditional on the data (FIA), as proportional to the likelihood of the data (based on *Hist*) multiplied by the prior(s):

$$p(\boldsymbol{\theta}|FIA) \propto p(FIA|r(\boldsymbol{\theta}), H(\boldsymbol{\theta}), \Delta r(\boldsymbol{\theta}), \Delta H(\boldsymbol{\theta})) \cdot p(\boldsymbol{\theta}) \quad (10)$$

Note that $\boldsymbol{\theta}$ represents the vector of 32 ACGCA model parameters (we use bold font to explicitly refer to the *vector* of parameters). The term

$p(\boldsymbol{\theta}|\text{FIA})$ is the posterior distribution of $\boldsymbol{\theta}$ conditional on the FIA data; $p(\text{FIA}|r(\boldsymbol{\theta}), H(\boldsymbol{\theta}), \Delta r(\boldsymbol{\theta}), \Delta H(\boldsymbol{\theta}))$ is the likelihood of the FIA data given the ACGCA outputs for r , H , Δr , and ΔH , which are deterministic functions of $\boldsymbol{\theta}$; and $p(\boldsymbol{\theta})$ is the joint prior for $\boldsymbol{\theta}$.

The likelihood of the FIA data was computed by evaluating *Hist* at the ACGCA output (r , h , Δr , Δh). In particular, for each annual time step ($t = 1, 2, \dots, T$) for which ACGCA outputs are produced, the likelihood is computed as:

$$p(\text{FIA}|r(\boldsymbol{\theta}), H(\boldsymbol{\theta}), \Delta r(\boldsymbol{\theta}), \Delta H(\boldsymbol{\theta})) = \prod_{t=1}^T \text{Hist}(r_t(\boldsymbol{\theta}), H_t(\boldsymbol{\theta}), \Delta r_t(\boldsymbol{\theta}), \Delta H_t(\boldsymbol{\theta})) \quad (11)$$

That is, for a vector of outputs for r , H , Δr , and ΔH (where $\Delta r_t = r_t - r_{t-\Delta t}$ and likewise for ΔH), at each time, t , we find the four-dimensional bin in *Hist* that contains these values, and we return the probability of observing this vector based on the relative frequencies of the FIA data that are looked up in *Hist*. Eq. 11 thus obtains the (histogram) probability of each simulated (r , H , Δr , ΔH) over the simulation period from initial year $t = 1$ to final year $t = T$, and the product of these probabilities is the likelihood of the data given the particular outputs produced by the ACGCA model for a given vector of parameters ($\boldsymbol{\theta}$). If the ACGCA simulation associated with a particular vector of trait values ($\boldsymbol{\theta}$) resulted in a tree that was in the healthy state for the entire 50-yr simulation, then $T = 50$ (approximately the average age of a tree in the FIA data). If the tree died during the simulation period (not in the healthy state), or had values outside of the minimum and maximum values set by *Hist*, the parameters were rejected in the MH algorithm (see *MH implementation*), because the likelihood is defined as 0 in these cases.

The prior, $p(\boldsymbol{\theta})$, in Eq. 10 is computed as the product of 32 independent univariate priors for each trait q in the parameter vector $\boldsymbol{\theta}$; that is,

$$p(\boldsymbol{\theta}) = \prod_{q=1}^{32} p(\theta_q)$$

where the priors for each θ_q are given in Appendix S1: Table S1. As noted previously, all parameters were log- or logit-transformed, and each is assigned a normal or truncated normal prior (see Eq. 13). For the normal priors:

$$\log(\theta_q) \text{ or } \text{logit}(\theta_q) \sim \text{Normal}(\overline{\theta}_q, \sigma_q) \quad (12)$$

Eq. 12 applies to all but four parameters in $q = 1, \dots, 32$; $\overline{\theta}_q$ and σ_q represent the prior mean and standard deviation, respectively, on the corresponding log or logit scale (see Appendix S1: Table S1).

Truncated normal priors were used for the other four parameters, η , η_B , H_{max} , and ρ (see Table 1 for definitions and Appendix S1: Table S1 for transformations), to exclude unrealistic or extreme values:

$$\log(\theta_q) \text{ or } \text{logit}(\theta_q) \sim \text{TruncNormal}(\overline{\theta}_q, \sigma_q, a_q, b_q) \quad (13)$$

where $\overline{\theta}_q$ and σ_q are the prior mean and standard deviation, and a_q and b_q are the lower and upper bounds, respectively. Both trunk-tapering parameters, η and η_B , were given bounds relative to each other such that $\eta > \eta_B$. This was accomplished by setting $a = \log(\eta_B)$ and $b = \infty$ for η , and $a = -\infty$ and $b = \log(\eta)$ for η_B . The maximum potential tree height on the log scale, $\log(H_{max})$, was given a lower bound of $a = -\infty$ and an upper bound of $b = \log(127 \text{ m})$ based on physical limitations of water transport (Domec et al. 2008). Finally, wood density, ρ , was given bounds based on physical (or engineering) constraints imposed by γ_X (Table 1), γ_w and $VwVc$, where $VwVc$ represents the volume ratio of structural tissue to internal cell volume for living sapwood cells such that:

$$a = \frac{VwVc - \gamma_X(VwVc - \beta)}{\gamma_w(1 + VwVc)} \quad (14)$$

$$b = \frac{1 - \gamma_X}{\gamma_w} \quad (15)$$

Eq. 14 is based on the assumption that there is a lower limit to the ratio of xylem cell wall area—mostly cellulose with density $1/\gamma_w$, where γ_w is assumed known (Suzuki 1999, Ogle and Pacala 2009)—to xylem conduit lumen area (set by β). Eq. 15 is based on the assumption that the conduit lumens do not contain structural tissue, and thus do not contribute mass to the bulk wood density. Here, we assume $VwVc = 0.5$, $\beta = 0.05$, and $\gamma_w = 6.67 \times 10^{-7} \text{ m}^3 \text{ g/dw}$, and we treat γ_X as unknown parameter (trait).

The above Bayesian model is relatively simple and does not involve any hierarchical priors. No attempt was made to estimate individual-, site-, or species-specific parameters. Instead, the goal of the Bayesian model is to yield distributions of the “global” θ vectors that are consistent with the “aggregated” FIA data—pooled across all individuals, sites, and species—and the semi-informative priors, which are also pooled across all studies (publications) and species. This greatly simplifies the model formulation and computational requirements (i.e., the ACGCA model is only run once for every θ vector, and the likelihood only needs to be evaluated once for a given ACGCA output vector at each simulation year). Hence, the posterior distribution of θ can be viewed as the probability distribution of trait values leading to realistic tree growth of healthy trees, across all species and environments combined. That is, the posterior marginalizes over individuals, sites, and species, such that posterior distributions for any individual, site, or species are expected to be contained within the aggregated distribution. Importantly, this approach eliminates combinations of trait values (θ vectors) that produce growth dynamics inconsistent with the FIA data (“unrealistic” growth).

As described above, *Hist* was used for the likelihood rather than an alternative distribution such as a multivariate normal or a kernel density estimate of the four-dimensional distribution. Both of these alternative approaches were explored, but they led to greater computational expense and/or undesirable behavior of the MH algorithm (see *Metropolis-Hastings algorithm*). Use of *Hist* greatly reduced the computational demands because it only needed to be computed once and then referenced via a “look-up” function when running the MH algorithm. The resulting simple, global analysis allowed us to run the MH algorithm on a desktop computer in a reasonable amount of time (~2 d).

Metropolis-Hastings algorithm

We implemented an MH algorithm to allow simultaneous evaluation of the ACGCA model and to compare the ACGCA output against *Hist*. Our MH algorithm for sampling from the posterior distribution is standard and follows Gelman et al. (2014). In summary, the algorithm proposes a vector of potential parameter values at each MH

iteration z and accepts or rejects the proposed parameters. In particular, let θ^* denote the proposed vector of parameter values, and let r_t^* , H_t^* , Δr_t^* , and ΔH_t^* denote the corresponding ACGCA outputs at simulation year t , given θ^* proposed at iteration z . We obtain θ^* by independently generating individual θ_q^* (again, for $q = 1, 2, \dots, 32$ components) from a jumping distribution, $J_z(\theta_q^*|\theta^{z-1})$. Truncated normal jumping distributions were employed for parameters with truncated priors (i.e., η , η_B , H_{max} , and ρ), using the same upper and/or lower limits as the priors (Eq. 13). Normal jumping distributions were used for all other θ_q^* .

As each component (θ_q^*) is proposed, it is either accepted or rejected based on the following acceptance ratio (ar_q) that involves evaluation of the posterior distribution (density), up to some normalizing constant (see Eq. 10), and the jumping distribution:

$$ar_q = \frac{p(\theta_q^*|FIA)/J_z(\theta_q^*|\theta^{z-1})}{p(\theta_q^{z-1}|FIA)/J_z(\theta_q^{z-1}|\theta^*)} = \frac{p(\theta_q^*|FIA) J_z(\theta_q^{z-1}|\theta^*)}{p(\theta_q^{z-1}|FIA) J_z(\theta_q^*|\theta^{z-1})} \quad (16)$$

If $ar_q > 1$, the posterior density evaluated at θ_q^* is greater than the posterior density at θ_q^{z-1} , and θ_q^* is accepted such that $\theta_q^z = \theta_q^*$. If the proposed value decreases the posterior density ($ar_q < 1$), it is accepted with probability ar_q ; otherwise, $\theta_q^z = \theta_q^{z-1}$ (Gelman et al. 2014).

MH implementation.—The above MH algorithm was applied to the ACGCA model and FIA data, for each of the aforementioned (11) light levels described in the ACGCA model section above. Five parallel MH chains were simulated for each of the 11 light levels (PAR_{max}), with PAR_{max} fixed at a single value for the duration of a given MH simulation. Starting values (at $z = 0$) for each parameter component, θ_q^0 , were generated for each chain by randomly sampling from the prior distributions. Starting values were rejected if they resulted in a zero likelihood according to *Hist* (Eq. 11); that is, we continued to randomly draw starting values until we obtained values that produced realistic growth curves (i.e., associated with positive probability in *Hist*).

Once acceptable starting values were obtained, jumping distributions for each MH chain were

tuned for 30,000 iterations to achieve near optimal acceptance rates of ~44% (Gelman et al. 1996). The simulations were executed for an additional 50,000 iterations after tuning, the first 20,000 of which were discarded as burn-in, yielding a sample of 30,000 iterations per chain. Thus, we obtained a total of 1,650,000 (5 chains \times 11 light levels \times 30,000 iterations) parameter sets overall, which we thinned by 50 to reduce both within-chain autocorrelation and storage requirements ($n = 33,000$ samples). We verified convergence of these thinned, post-burn-in chains using the Gelman diagnostic tool (Plummer et al. 2006) in R (see Appendix S2). All results refer to the thinned output unless otherwise noted.

All MH code for the analysis was written in the R programming language (R Core Team 2015), and the ACGCA model was programmed in C based on code developed by Ogle and Pacala (2009) and Gemoets et al. (2013). A wrapper function in C was written to pass inputs from R to the C code (Gemoets et al. 2013), and return outputs to R. This code was then implemented via a custom parallelization algorithm allowing multiple R sessions to run simultaneously, each running a single chain.

Output analysis

Sensitivity analysis.—Again, we only used FIA data for trees that are assumed to be healthy and growing; we do not explicitly account for various filtering processes (e.g., non-light-related environmental stress or competition), but we impose mass-balance and engineering constraints contained within the ACGCA model. Thus, we interpret the joint posterior distribution of the parameters, θ , as the TTS. First, we use the TTS to explore the sensitivity of tree growth to changes in the TTS traits. Using $n = 3300$ θ vectors from the TTS (obtained by retrieving every 10th sample from the 33,000 vectors), we obtained the predicted (output) radius (r) and height (H) values, and we computed growth rates (Δr and ΔH) representative of “young” (simulation years 1–10) and “mature” (years 41–50) trees. For each of the four growth indices, we regressed the predicted growth index (y variable) on the corresponding parameters (traits, x variables) that produced the growth index. This was accomplished in R using the linear model (`lm`) function where y was regressed on all x

variables (32 traits), including main effects and quadratic effects of each trait, and all two-way interactions among traits; consider this the “full” model. Next, we repeated the regression analysis 32 times, whereby one of the traits (x variables) was removed; consider these the reduced models. Then, for each trait, we computed the partial R^2 based on the difference in the sum of squared errors (residuals) between the full and reduced model (Kutner et al. 2005). Higher partial R^2 (maximum = 1) values indicate greater importance of a trait for predicting growth, relative to traits associated with lower values.

Posterior parameter space.—To evaluate the structure of the TTS, independent of predicted growth, we graphically explored whether the TTS is refined compared to the independent prior distributions used for each trait. To initially address this, we overlaid the marginal posterior distributions for each θ_q (each trait) with the corresponding prior distribution for that trait. Next, we analyzed the posterior samples of θ to explore trait correlations (or trade-offs) associated with the TTS by computing bivariate correlations between all unique pairs of the 32 θ_q , yielding $(32 \times 31)/2 = 496$ bivariate plots and associated Pearson correlation coefficients.

To further explore the correlation structure of the TTS, as contained in the posterior samples, we evaluated how perturbations to this structure affect tree growth. For these simulations, the posterior samples of the individual θ_q , for all 11 light levels, were stored in a 33,000 (MH iterations) \times 32 (parameters) matrix that maintained the correlation structure produced by the MH simulations. This correlation structure was subsequently perturbed such that, for a given column (or trait, q), all of the sampled values (rows) were randomized without replacement, producing a new matrix of parameter values. This was repeated for each column (parameter), while maintaining the original row (iteration) order of the other 31 columns (parameters). Thus, we produced 33 matrices of posterior samples; one maintained the original correlation structure, and the others (32) maintained the correlation structure of all but one of the parameters (or traits). For each of these 32 randomized parameter matrices, the ACGCA model was run for each of the 33,000 rows (each containing a randomized parameter vector), resulting in associated output vectors (r ,

H , Δr , and ΔH). The likelihood of each output vector was evaluated with Eq. 11 (*Hist*) to determine whether the corresponding, randomized parameter vector produced realistic tree growth (i.e., a likelihood >0), indicating that the simulated tree survived for 50 yr, remained in a healthy state, and was not associated with unrealistic values for r , H , Δr , and/or ΔH . From these simulations, we calculated, across all light levels, the proportion of the “new” (randomized) 33,000 parameter vectors that produced realistic tree growth, for each of the 32 matrices for which one trait was randomized.

Multivariate trait correlation structure.—The above randomization of individual trait values suggested a more complicated correlation structure among the 32 traits that was not revealed by the bivariate analyses (see *Results*). Thus, we conducted multiple regressions to further assess the correlation structure of the TTS defined by the joint posterior for θ . The rationale for the regressions was to consider the MH posterior samples as a dataset, and then to treat each of the 32 traits (θ_q) in turn as the dependent variable with the remaining 31 traits and light level serving as 32 independent (explanatory) variables. Each trait, whether treated as the independent or dependent variable, was log- or logit-transformed according to the transformation used in the Bayesian model (see Appendix S1: Table S1). The transformed values were standardized by subtracting their posterior mean and dividing by their posterior standard deviation. We refer to each transformed and standardized parameter (trait) as δ_q , all of which are unitless, with mean 0 and variance 1. For consistency, light level was rescaled from -3 (lowest light level) to $+3$ (highest level), roughly the same range as the standardized traits (δ_q).

We conducted stepwise regressions in R by fitting two models for each trait: one with only main effects, and one with main effects and all possible two-way interactions. All stepwise regressions used forward and backward selection. The Bayesian Information Criterion (BIC) was used for model selection because it tends to select more parsimonious models compared to the Akaike information criterion (AIC) given that BIC’s penalty term is larger per variable added for large datasets (Gelman et al. 2014).

Results from stepwise regression allowed exploration of the importance of trait–trait interactions for understanding the “overall” effect of one trait on another trait. For example, consider the following generic regression model for dependent variable trait δ_q , which is significantly correlated with independent variable traits δ_i and δ_j and their interaction ($q \neq i$ or j):

$$\delta_q = \beta_0 + \beta_i \delta_i + \beta_j \delta_j + \beta_{ij} \delta_i \delta_j \quad (17)$$

The overall effect of δ_i is given by combining all terms on the right-hand side involving δ_i and factoring out δ_i , such that Eq. 17 can be rewritten as:

$$\delta_q = \beta_0 + (\beta_i + \beta_{ij} \delta_j) \delta_i + \beta_j \delta_j \quad (18)$$

Thus, the overall effect of δ_i (i.e., $\beta_i + \beta_{ij} \delta_j$) depends on the partial regression coefficients for its main effect (β_i) and interaction term (β_{ij}) and the value of the other trait, δ_j . Because the regression variables (δ) are linear transformations of the actual trait (θ), Eq. 18 allowed us to quantify how correlations between pairs of traits depend on the values of other traits. Thus, interactions with other traits could potentially result in a wide range of possible bivariate correlations (negative, uncorrelated, or positive) and strengths of correlations (strong to weak) between two traits (e.g., θ_q and θ_i), conditional on the values of other traits (e.g., θ_j).

We used Eq. 18 to approximate the posterior distributions for the overall effects for each dependent trait. That is, for each of the 32 dependent trait models, Eq. 18 was evaluated at the point estimates of the regression coefficients (β ’s), for every posterior parameter vector ($n = 33,000$) of the associated independent traits (e.g., δ_i [or θ_i] and δ_j [or θ_j] in Eq. 18). This approach ignores uncertainty in the regression coefficients (β), but it does account for uncertainty in and covariation among the traits, as quantified by the joint posterior for θ .

RESULTS

ACGCA model vs. FIA comparison

The posterior region of the ACGCA simulations for tree radius vs. height generally had good overlap with the FIA data (Fig. 1a, b). Since

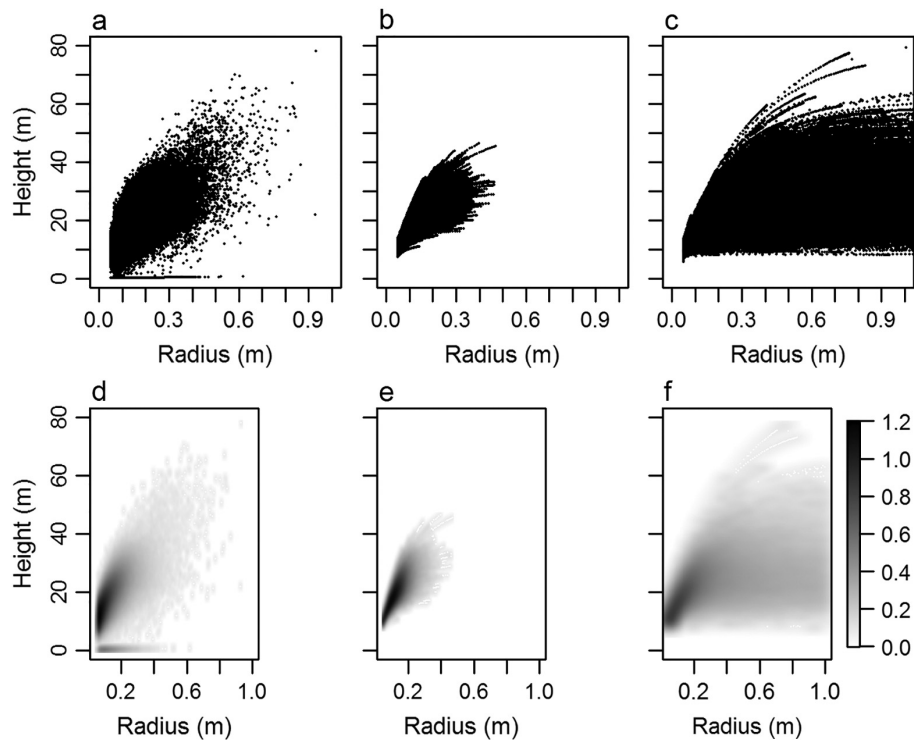


Fig. 1. Tree height (H) vs. trunk radius (r) based on (a) Forest Inventory and Analysis (FIA) data only ($n = 1,270,510$ data points), (b) the ACGCA model after having fit the model to the FIA data ($n = 1,650,000$ simulations points), and (c) the ACGCA model based on prior distributions (no FIA data), whereby parameters (traits) are randomly drawn from the independent priors and only growth curves representing “healthy” trees are kept ($n = 1,650,000$ simulation points). The bottom panels d–f show the same height vs. radius relationships but as smoothed color density plots.

the ACGCA model was only run for 50 years in each simulation, it did not reach the large radii and heights reported for trees from older stands. The ACGCA model also did not sufficiently capture the FIA region characterized by short trees with small radii, perhaps because these trees may not align with the ACGCA model’s “healthy” condition. However, the growth curves (and associated parameter or trait values) obtained by fitting the ACGCA model to the aggregated FIA data (Fig. 1b, e) are notably refined (more constrained) relative to the growth curves produced by the ACGCA model in the absence of the FIA data (Fig. 1c, f).

Posterior parameter samples

Posterior estimates for θ are given in Appendix S1: Table S2. For 30 of the 32 θ_q ’s (traits), the 95% posterior credible intervals (CIs)

included the prior mean, for each of the 11 light-level-specific marginal distributions. Based on visual inspection, the posteriors closely resembled the priors for 18 of the θ_q ’s (as in Fig. 2c; for 12 θ_q ’s, the posteriors were not notably different from the priors, but were slightly shifted (as in Fig. 2b); for only two θ_q ’s (ϵ and S_O), the posterior and prior distributions were notably different (as in Fig. 2a). For S_O , the posteriors did not differ by light level, but the overall posterior mean and 95% CI were 0.13 [0.01, 0.47] year^{-1} , resulting in a slower senescence rate (longer lifespan) for stems and coarse roots (“other” woody tissue) compared to what would be predicted from the literature (prior mean = 1.85 yr^{-1} ; Appendix S1: Fig. S1). Only one parameter (ϵ , radiation-use efficiency) had posterior distributions that noticeably differed across light levels (Fig. 2a). The four highest light levels

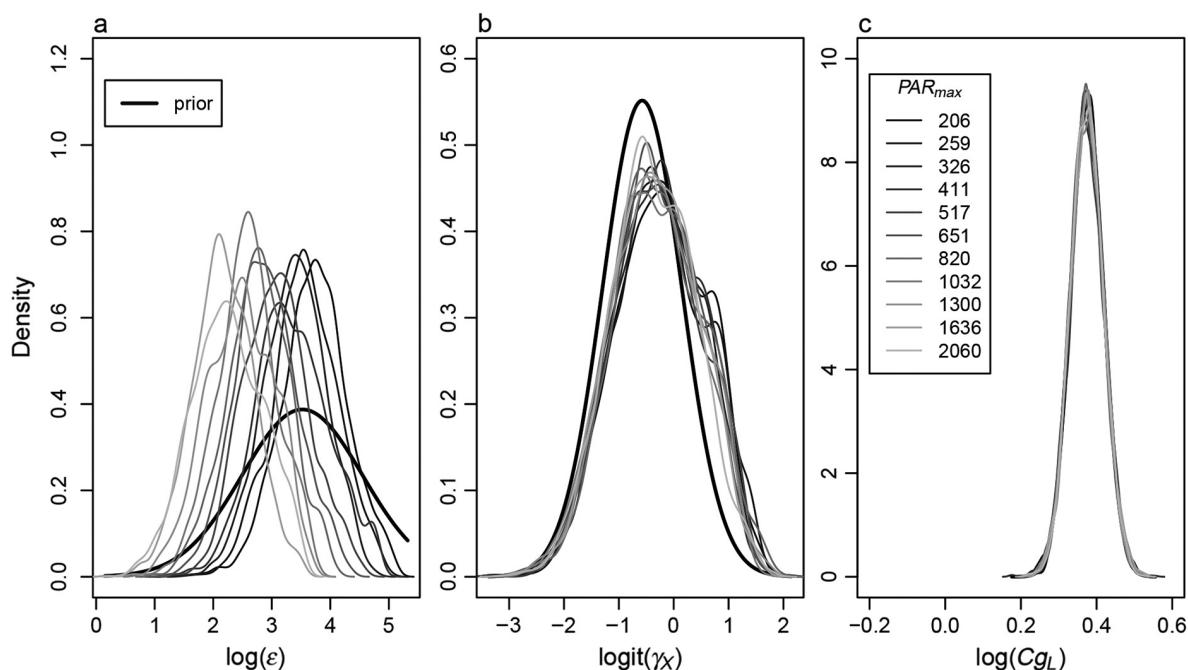


Fig. 2. Marginal posterior probability densities by light level (11 thin lines) for a select set of parameters (traits), overlaid with their prior probability distributions (thick black lines) for transformed values of (a) radiation-use efficiency (ϵ , g gluc/MJ), (b) proportion of xylem conducting area (γ_X , unitless), and (c) construction cost of producing leaves (C_{gL} , g gluc/g/dw). Three main patterns emerged across the 32 traits: (a) shows the only case of notable differentiation of the posterior by light level, and it also illustrates differences between the prior and posteriors— S_O was the only other parameter (trait) where the posterior visually differed from the prior; (b) shows that the posterior distributions obtained under the 11 light levels were nearly identical, and the prior and posteriors were only slightly differentiated for, but effectively very similar for one γ_X of 11 traits (several other traits showed a similar pattern: H_{max} , SW_{max} , ρ , f_L , f_2 , γ_X , R_{mL} , R_{mS} , R_{mR} , η_B , R_0 , R_{40}); and (c) shows one (C_{gL}) of 18 traits described by a high degree of overlap between the prior and posterior distributions (other traits with a similar pattern: ϕ_H , η , λ_S , λ_H , γ_C , C_{gR} , C_{gW} , δ_L , δ_R , S_L , SLA , S_R , r_R , ρ_R , k , m , α). See Table 1 for definitions of traits (parameters).

(PAR_{max} = 50, 63, 79, and 100% of maximum light) resulted in posterior means and 95% CIs for ϵ that varied from 15.0 [4.8, 35.0], 13.6 [3.7, 31.4], 9.9 [3.0, 24.4], to 11.3 [2.9, 28.8] g gluc/MJ, respectively. These posterior estimates were significantly different from the prior mean (37.81 g gluc/MJ) and showed a trend of decreasing ϵ as PAR_{max} increased (Appendix S1: Fig. S2).

Bivariate relationships

Bivariate correlations among all possible pairs of the θ_i 's (496 total pairs) were generally weak (Appendix S1: Table S3); for example, only 178 pairs were associated with significant ($P \leq 0.05$) correlations, ranging from Pearson correlations of $R = -0.25$ to 0.42. The remaining 175 correlations may be deemed biologically insignificant

given that $|R| < 0.2$, but many of these were still statistically significant (Appendix S1: Table S3) due to the large number of posterior samples used to compute R .

Starting values and resampling

Generation of starting values required an average (based on $n = 10$ repetitions of generating starting values for each light level) of 7004 (32% light) to 52,353 (100% light) draws from the priors to obtain a single vector of starting values for θ , with an overall mean (across all 11 light levels) of 24,996 draws ($n = 110$; Table 2). The high number of draws required to generate starting values indicates that many parameter sets lead to unrealistic tree growth, such that the simulated tree heights and radii fell outside the empirical

Table 2. The mean number of draws from the priors required to obtain a parameter vector, θ , that resulted in realistic tree growth under each light level depicted by the PAR_{max} values (mean and standard deviation [SD] based on $n = 10$ simulations).

Mean no. draws	SD	PAR_{max}
43235.9	38392.1	206
13806.3	10946.8	259
21053.3	24366.2	326
14530.5	9413.5	411
7041.2	4834.6	517
7004.3	7448.3	651
13958.7	7711.6	820
29815.2	31777.0	1032
26828.7	16398.4	1300
45324.5	37804.6	1636
52352.8	56124.9	2060

Note: For example, when $PAR_{max} = 206 \text{ MJ}\cdot\text{m}^{-2}\cdot\text{yr}^{-1}$, over 43,000 random draws from the priors are generally required to find a single set of parameter values that lead to predicted r , H , Δr , and ΔH associated with a probability >0 given the FIA histogram (*Hist*).

distribution estimated from FIA data (as determined by *Hist*).

The resampling procedure for evaluating the importance of the parameter correlation structure, as quantified by the MH posterior samples, resulted in acceptance rates from 13.4% (when radiation-use efficiency, ϵ , was randomized relative to the other traits) to ~100% (when labile carbon storage capacity of leaves, δ_L , or roots, δ_R , was randomized; Fig. 3). Randomization of four other parameters (traits) led to acceptance rates lower than 50%: maximum potential crown radius of a tree with diameter at breast height of 40 cm (R_{40}), root and leaf maintenance respiration rates (R_{mR} and R_{mL}), and the fine root area to leaf area ratio (f_l ; Fig. 3).

Sensitivity analysis

The multiple regressions of the four different growth indices—radial and height growth, for young and mature trees—on the 32 traits

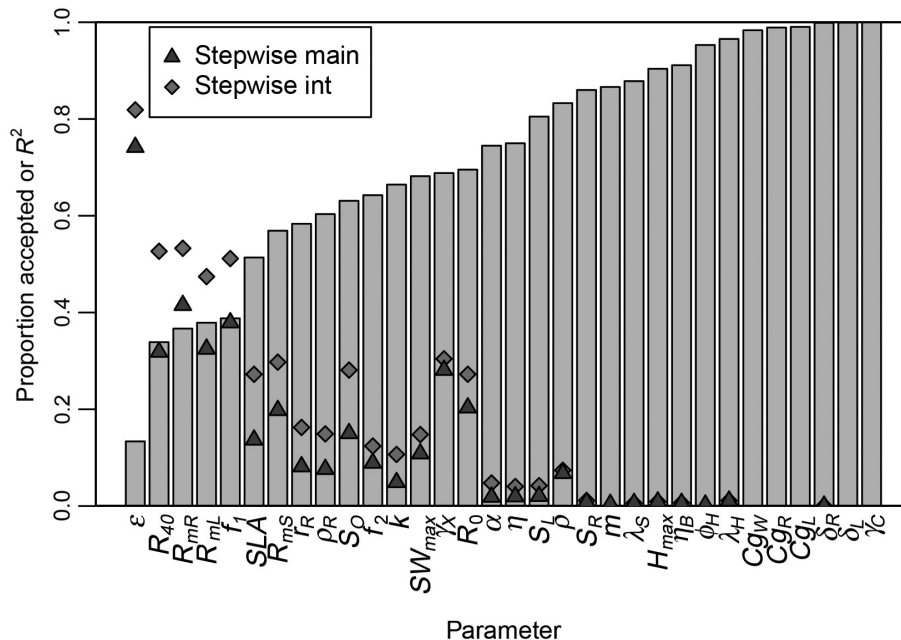


Fig. 3. The proportion of values accepted after randomizing the order of each parameter with respect to MH iteration number (gray bars) overlaid with the R^2 values associated with two different stepwise regressions (points) that treated each parameter as the dependent variable: stepwise regressions with main effects only (triangle) or main effects and two-way interactions (diamond). In general, R^2 values increased as the proportion accepted increased. In some cases (for parameters such as R_{40} , R_{mR} , R_{mL} , f_l , SLA , and S_O), it is clear from the stepwise regressions that including interactions drastically improved model fit. However, there were often many more variables in these models (for SLA , 23 terms in the main effects-only model vs. 116 in the model with main effects and interactions). See Table 1 for definitions of the parameters.

revealed that similar traits govern height and radial growth and that growth is insensitive to many of these traits. Radial and height growth of young trees was most sensitive to R_0 , ϵ , S_O , f_1 , R_{mR} , and R_{mL} ; only two of these traits (S_O and R_0) were also among the top predictors of growth in mature trees, which was also sensitive to γ_X , R_{mS} , f_2 , and R_{40} (partial R^2 values >0.1 for both growth indices; Fig. 4a, b). Growth of

young trees was insensitive to Cg_R , Cg_W , λ_S , S_R , δ_R , δ_L , and γ_C , and growth of mature trees was also insensitive to Cg_R , Cg_W , S_R , and δ_L , in addition to η , M , and Cg_L (partial R^2 values <0.02 ; Fig. 4a, b). See Table 1 for trait definitions.

Multiple-regression results

Stepwise regressions, with and without two-way interactions, produced statistically significant

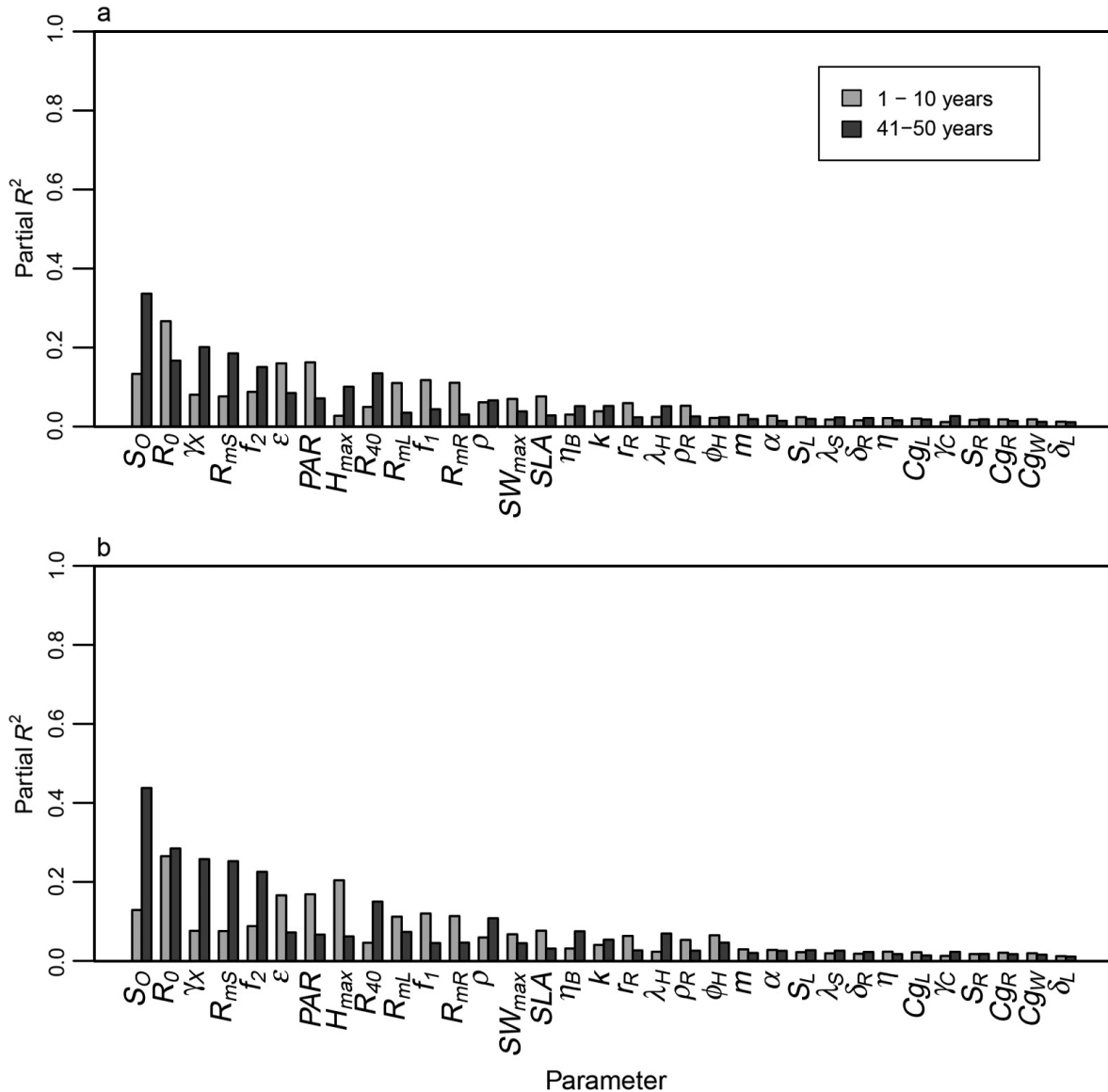


Fig. 4. Partial R^2 values from the sensitivity analysis for traits in regression models explaining change in radius (a) and change in height (b) for two time periods: years 1–10 (“young” trees, light gray bars) and years 41–50 (“mature” trees, dark gray bars). Higher partial R^2 values indicate greater importance of that trait for predicting growth. See Table 1 for definitions of traits (parameters).

models ($P < 0.05$), with coefficients of determination (R^2) as high as 0.81 (stepwise with interactions) when ε was treated as the dependent variable (Appendix S1: Table S4; Fig. 3). Many models with low R^2 (e.g., H_{max} , $R^2 = 0.009$) were still statistically significant (e.g., $P \ll 0.01$) due to the large sample size ($n = 33,000$). The stepwise regression procedure that only considered main effects produced models only containing intercept terms when γ_C , C_{gL} , C_{gR} , C_{gw} , and δ_L were treated as the dependent variable. When the procedure included two-way interactions, it produced models only containing intercepts for the aforementioned variables, in addition to φ_H and m (see Table 1 for trait definitions). In these cases, no relationship was identified between the aforementioned “dependent variable” traits and other “independent variable” traits. As expected, models for these traits yielded the smallest R^2 values, and when these traits were randomized, they had high acceptance rates in the resampling procedure (Fig. 3), and they were associated with many low, non-significant bivariate correlations (Appendix S1: Table S3).

Across the 32 different θ_q 's, the R^2 values from the different stepwise regression models increased as the acceptance rate from the resampling procedure decreased (Fig. 3; Appendix S1: Table S4). Adding two-way interactions in the stepwise regressions greatly increased the R^2 for some models (traits); for example, when two-way interactions were included, the R^2 for the model of R_{40} increased from 0.32 (main effects only) to 0.53, but was accompanied by a large increase in the number of model parameters, from 21 to 114 (Appendix S1: Table S4). The increase in parameters when including two-way interactions was driven by the inclusion of a large number of interaction terms, and occasionally an additional main effect (Fig. 5; Appendix S1: Table S4). The direction (positive or negative) of the main effects was generally not changed by adding interactions.

The trait models with the highest R^2 values were the same for the stepwise regressions both with and without two-way interactions. The top five models with the highest R^2 values corresponded to the models for ε , R_{mR} , f_L , R_{mL} , and R_{40} , with R^2 values of 0.74, 0.42, 0.38, 0.33, and 0.32 (main effects only), respectively, and 0.82, 0.53, 0.51, 0.48, and 0.53 (main effects and interactions), respectively. It

is worth noting that of these traits, R_{mL} is part of the LES (Wright et al. 2004) and ε is related to the LES via its relationship to leaf N (Sinclair and Horie 1989, Wang et al. 1991, Martin and Jokela 2004). The model for SLA —an important LES trait—had R^2 values of 0.28 (with interactions) and 0.14 (without interactions). With respect to the WES, ρ is the only ACGCA parameter that is explicitly included in the WES; the models for ρ had low R^2 values (e.g., $R^2 = 0.07$ with interactions). However, γ_X is indirectly related to the WES, and it had the sixth highest R^2 (0.31 with interactions). In general, the traits (θ_q 's) that were associated with models with relatively high R^2 values were also typically included as predictors in models for other traits and were included in more interactions (Fig. 5; Appendix S1: Table S4). Further, traits that are directly or indirectly related to the LES or WES were often included as predictors in regression models for other LES- or WES-related traits. For instance, the leaf traits SLA and R_{mL} were included as predictors of ε , and the wood traits R_{mS} and ρ were included as predictors of γ_X (Fig. 5).

Focusing on the stepwise regressions with two-way interactions, the overall effect of each independent variable trait (e.g., see Eqs. 17 and 18) shows that the correlation between the dependent (δ_q) and the independent variable traits can change when considering interactions with other traits (e.g., δ_j in Eqs. 17 and 18; Fig. 6). In some cases, the overall effect can switch signs relative to the main effect—for example, see the overall effect of R_{mS} (along x -axes) on ε (Fig. 6a), R_{mL} (Fig. 6b), and R_{mR} (Fig. 6c), depending on the values of the interacting traits. In most cases, the overall effect is primarily negative or positive, with the magnitude of the effect being influenced by interacting traits. For example, the main effect of ε on R_{mL} is 1.29 (Fig. 6b), but the approximated 95% CI representing the overall effect spans (0.06, 2.71).

DISCUSSION

Structure of the theoretical trait space

The TTS produced by the individual-based tree growth model (ACGCA), constrained by forest inventory (FIA) and literature (TreeTraits) data, suggests complex multivariate relationships among a subset of functional traits related to tree growth and carbon allocation. Bivariate, trait-trait correlations were generally weak within the

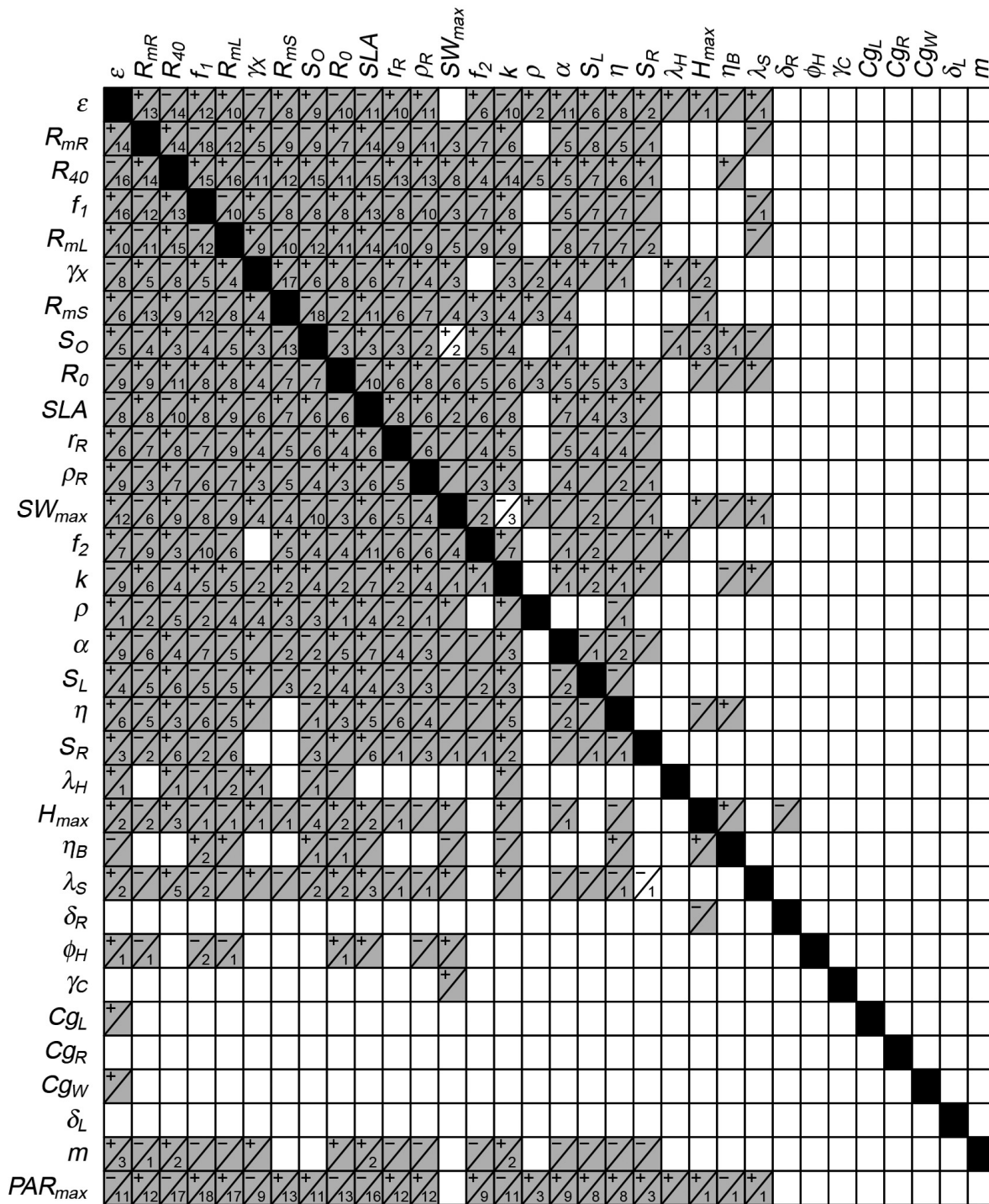


Fig. 5. Summary of effects included in multiple-regression models found with a stepwise regression routine including main effects and all two-way interactions. Each column represents a model (i.e., columns are associated with the trait that as treated as the dependent variable), and each row represents a potential covariate in the model. When appropriate, ± in a cell indicates the direction of the main effect for a given variable. The number under each diagonal line in a cell represents the number of interaction terms that the corresponding covariate

(Fig. 5. *Continued*)

trait was included in; if left blank, then it only occurred as a main effect. Gray shaded cells denote statistically significant main effects ($P < 0.05$, most $P \ll 0.05$); all interaction effects were statistically significant, all but three main effects were statistically significant, and the three non-significant main effects were included in at least one significant interaction within the corresponding model. All parameters were transformed according to Appendix S1: Table S1 and normalized. PAR_{max} ($\text{MJ}\cdot\text{m}^{-2}\cdot\text{yr}^{-1}$) is light level, which is treated as a fixed driving variable and is not a functional trait.

TTS (Fig. 7; Appendix S1: Table S3). Yet, it is clear from evaluation of the data-constrained ACGCA output (posterior for θ) that about half of the 32 traits (θ_q 's) cannot be randomly combined; specific combinations of traits are necessary to achieve predictions of realistic tree growth. This is further emphasized by drawing values of each θ_q (trait) from the independent, literature-based marginal priors; the majority of trait value combinations are rejected because they lead to growth patterns that either do not agree with the FIA data (Table 2) or lead to an unhealthy state given the ACGCA model structure. For example, most cases of randomly drawn trait combinations resulted in trees that died during the simulation, with most dying during the first time step. Similarly, the results from independently randomizing each trait (θ_q ; Fig. 3) within the joint posterior (TTS) clearly show that the TTS contains important correlation structure that is necessary to produce realistic predictions of tree growth. Taken together with the stepwise regressions, our findings provide evidence for complex, multi-dimensional relationships between a subset of functional traits that govern tree growth in the TTS, but tree growth is insensitive to the other (ca. half) traits in the TTS.

We find it interesting that only a subset of traits exhibited complex, contingent relationships (e.g., ε , R_{mR} , f , R_{mL} , γ_X , R_0 , R_{mS} , SLA , and a few others; Figs. 3, 5); these traits are also the best predictors of radial and height growth (Fig. 4). Somewhat surprising, tree growth is relatively insensitive to about half of the 32 traits (e.g., δ_L , C_{gL} , C_{gW} , C_{gR} , γ_C , S_R , S_L , and η , among others; Fig. 4), and these are also the traits that are expected to operate independent of each other in the TTS (e.g., Figs. 3, 5), or that are not directly informed by the FIA data on tree radii and heights. This implies that a smaller (ca. 15–16) set of traits are important for understanding how tree growth responds to light, the environmental driver considered here. Thus, while coordination

may occur among certain traits in response to specific environmental limitations, other traits may be irrelevant. In this study, only light was included as an environmental driver; if another driver, such as water availability, were included, tree growth would likely be sensitive to a different subset of traits.

Relationships between traits and the importance of under-represented traits

Multiple-regression analysis of the TTS provided insight into relationships among traits and between traits and light level. Of the subset of coordinated traits revealed by our analyses, we focus on traits that are frequently measured in field or laboratory settings and that are related to empirical trait spectra (e.g., LES, WES). For instance, when SLA was treated as the dependent variable trait, it was positively related to leaf maintenance respiration (R_{mL}), as expected (Wright et al. 2004), and negatively related to light level (PAR_{max}), in agreement with previous work showing that SLA is up to two times higher for leaves produced in shade compared to high light (Evans and Poorter 2001, Ogle et al. 2013). Unanticipated relationships also emerged. For example, SLA was correlated with a number of root traits (R_{mR} , f_L , r_R , and ρ_r), many of which are often challenging to measure and could possibly define a root economics spectrum (Reich 2014). Other infrequently measured traits (e.g., R_0 , R_{40} , S_O) were often included as predictors of more frequently measured traits (e.g., SLA , R_{mL} , R_{mR} , ρ ; Fig. 5; see Table 1 for trait definitions). While it is often impractical, due to logistics or expense, to measure traits such as S_O (branch and coarse root senescence rate) and various root traits (Weiher et al. 1999, Lavorel et al. 2007), we demonstrate that modeling can help reveal potential relationships among traits that might otherwise be impractical to investigate. Although the trait relationships that emerge from our analysis are not directly equivalent to those

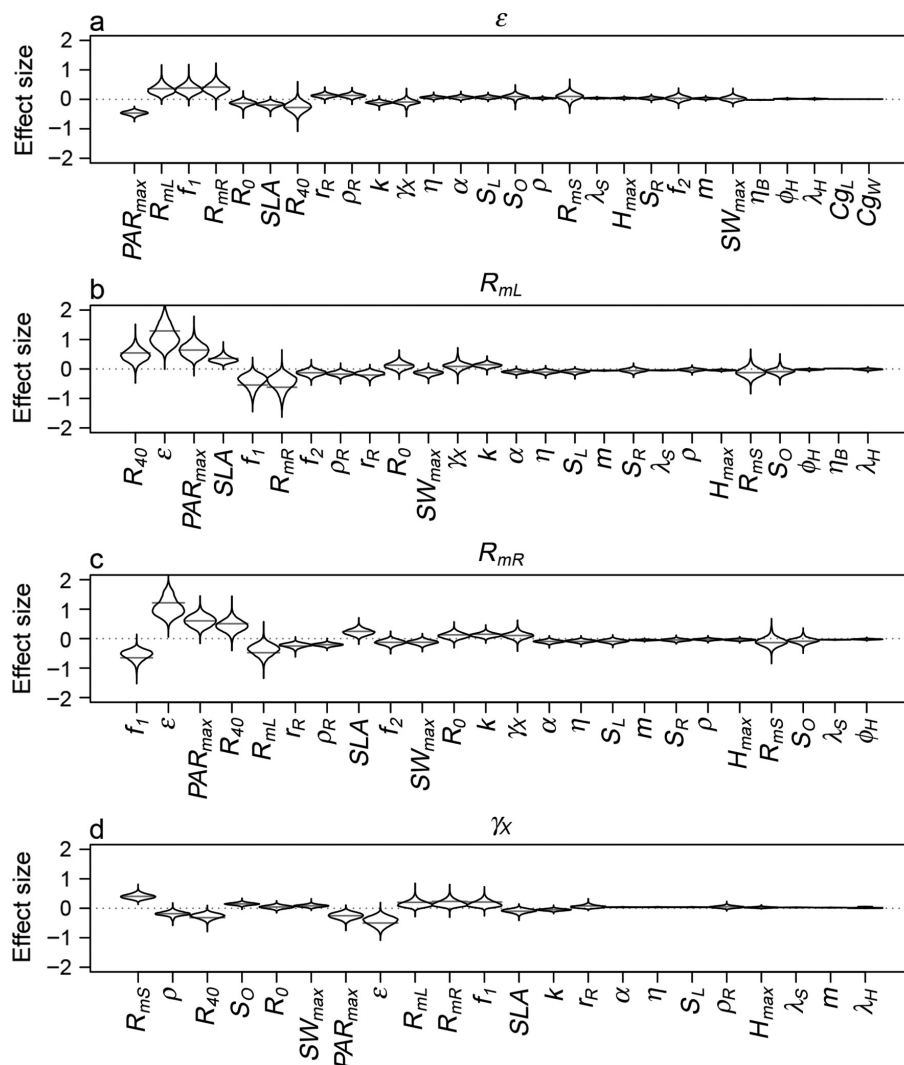


Fig. 6. Main effects of variables (traits) included in the stepwise regressions that treated the following four traits as dependent variables: (a) radiation-use efficiency (ϵ), (b) leaf maintenance respiration (R_{mL}), (c) fine root maintenance respiration (R_{mR}), and (d) proportion xylem conducting area (γ_x). In these regressions, the dependent traits and the independent traits (x -axes) were normalized such that the normalized variables are unitless. The violin plots show the overall main effect of each variable (on x -axes) when taking into account interactions (e.g., Eqs. 17 and 18), which contain the corresponding partial regression coefficient for the actual main effect (light gray horizontal lines). Three primary cases are illustrated: (1) The interactions lead to a variable overall main effect such that the violin plot is comparatively wide, but the direction of the overall effect is consistent with the partial main effect (negative or positive); (2) the overall main effect can shift from negative to positive, or vice versa, given the values of interacting variables (e.g., violin plots to overlap the dashed, horizontal zero line); and (3) the interactions have little influence such that the overall main effect is nearly indistinguishable from the partial main effect (e.g., very narrow violin plots). See Table 1 for definitions of the traits. All traits were transformed according to Appendix S1: Table S1 and normalized.

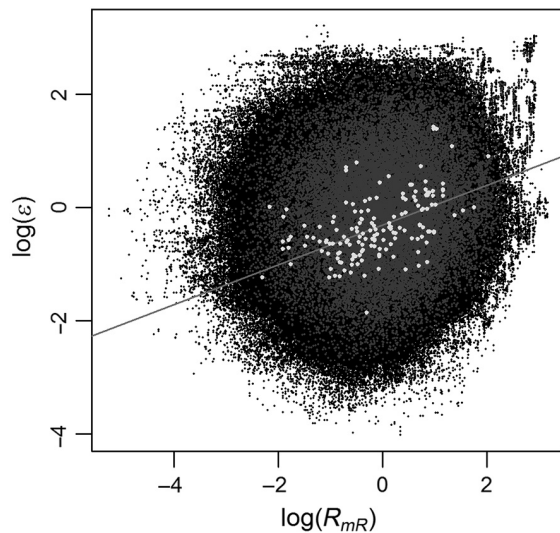


Fig. 7. Bivariate posterior plots for an example parameter (trait) pair ε and R_{mR} , radiation-use efficiency and root maintenance respiration, respectively. The black points are the 1.65 million parameter pairs generated by the MH routine before thinning by 50, and the dark gray points represent the subset of 33,000 points used to calculate posterior statistics. The light gray points represent a subset of the posterior space obtained by filtering the MH output such that the middle 20% quantile for PAR_{max} , f_{1L} , R_{mL} , R_{40} , and SLA was retained (all other samples ignored), resulting in 231 parameter sets out of 1.65 million that met these criteria; this filtering by other traits led to a significant Pearson correlation ($R = 0.26$, $P < 0.05$) between the focal pair of traits (ε and R_{mR}). All traits were transformed according to Appendix S1: Table S1 and normalized; see Table 1 for definitions of traits.

measured in the field that explicitly evaluate inter- and/or intraspecific relationships, the model-based TTS suggests that future observational or experimental studies should consider potentially important traits (e.g., R_0 , R_{40} , S_O , SW_{max} , f_{1L} , R_{mR} , R_{mS} ; see Table 1) that are under-represented in most measurement campaigns.

Additionally, for a subset of traits, their relationships (trade-offs) with other traits appear more complex than suggested by empirical studies. For example, while the bivariate correlation between light-use efficiency (ε) and root maintenance respiration (R_{mR}) is weak (Appendix S1: Table S3), R_{mR} is a significant predictor of ε when other traits are considered (e.g., f_{1L} , SLA , R_{mL} , R_{40}),

partly because of interactions between R_{mR} , these other traits, and light level (Fig. 5). Existing empirical trait spectra—including the LES (Wright et al. 2004), WES (Chave et al. 2009), and the worldwide fast–slow spectrum (Reich 2014)—typically do not evaluate trait–trait relationships beyond at most three traits (e.g., 3D plots). Studies using ordination methods provide an indication that interactions exist, in that multiple traits are often found to be correlated with a particular axis in the ordination (Cavender-Bares et al. 2004, Díaz et al. 2004, Baraloto et al. 2010, Stahl et al. 2013). The results from this study, however, indicate that explicit consideration of multiple trait–trait or trait–environment interactions is potentially important (Fig. 5). Considering the variety of relationships proposed in plant physiological models—such as photosynthetic models (Farquhar et al. 1980), water transport models (Sperry et al. 1998, Tuzet et al. 2003), stomatal conductance models (Ball et al. 1987, Damour et al. 2010, Medlyn et al. 2011)—it is perhaps unsurprising that multiple plant functional traits interact to govern lower dimensional trait spaces (e.g., bivariate trait relationships), especially when they are known to be correlated with the same underlying physiological processes.

We highlight potential mechanisms that may give rise to some of the trait–trait relationships that emerged through our multivariate analyses. These trade-offs result from a combination of constraints inherent to the structure of the ACGCA model as well as the constraints placed on tree growth by fitting the model to FIA and TreeTraits data. Consider one of the trade-offs that emerged for SLA that may be representative of a hidden mass conservation trade-off. To achieve a particular growth rate or size, as SLA increases for a fixed amount of leaf biomass, leaf area (LA) increases, which is expected to lead to increased photosynthesis (P_G). If more carbon is fixed, then this “excess” carbon must be incorporated into tissues, respired, or lost. Again, to achieve a particular (fixed) growth rate as SLA increase, this would require that the excess carbon be lost, which is reflected in the positive correlation between SLA vs. respiration (R_{mR} and R_{mL}) and/or tissue senescence (S_R and S_L ; Fig. 5). The negative correlation between γ_X and ρ may be interpreted as an engineering trade-off. For a fixed trunk radius, as the conducting area in the sapwood increases

(increase in γ_X), this leads to less structural tissue and lower overall wood density (ρ).

Independent or potentially irrelevant traits

The regression analyses of the TTS, however, suggest that a notable number of traits (~50% of the 32 explored here) are independent of all other traits, in agreement with our results from randomizing traits (Fig. 3). The randomization (Fig. 3) and sensitivity (Fig. 4) analyses utilized the trait values produced by fitting the ACGCA model to the FIA data, but they are otherwise independent of the FIA data and reflect inherent structure and constraints (e.g., engineering and mass-balance trade-offs) contained within the ACGCA model. Thus, these analyses point to this subset of “independent” traits as those traits that are essentially irrelevant for understanding tree growth, in terms of height and radial increment. These are also traits that appear to be uninformed by the FIA data given that they are uncorrelated with other traits, and their marginal posteriors mirror their independent priors. However, additional sensitivity analyses indicated that some of the traits that are irrelevant to growth are critical for predicting whole-plant labile carbon status (such as H_{max} , γ_C and η_B ; Fig. 4; Appendix S1: Fig. S4), which determines tree survival (Ogle and Pacala 2009). This implies that integration of survival data from the FIA database could help inform these traits.

In summary, our results suggest that potentially a small set of traits are necessary for understanding a particular integrated process (e.g., height growth, radial growth, survival), but that these trait subsets may differ depending on the process of interest. A similar result is reflected in empirical studies showing that traits making up the LES are often uncorrelated with traits in the WES, with the traits in each spectrum being related to different whole-plant processes (Baraloto et al. 2010).

Trade-offs from economics spectra

Our analysis did not reveal strong correlations or trade-offs between pairs of traits (Appendix S1: Table S3), in contrast to previously described trait spectra such as the LES and WES (Wright et al. 2004, Chave et al. 2009, Reich 2014). The stepwise regression results, however, provide evidence for the existence of such trait trade-offs in the TTS,

many of which agree with the empirical economics spectra. One example, mentioned above, is the relationship between SLA and R_{mL} (equivalent to R_{mass} in the LES). When SLA is treated as the dependent trait, the partial regression coefficient for R_{mL} is positive, which agrees with the relationship in the LES (Wright et al. 2004). The LES correlation between leaf lifespan ($LL = S_L^{-1}$) and LMA ($LMA = SLA^{-1}$) is positive (Wright et al. 2004), which agrees with the partial regression coefficient for S_L in the model for SLA . Likewise, R_{mL} and LL are positively correlated in the LES (Wright et al. 2004), which agrees with the negative partial regression coefficient for S_L (since $S_L = LL^{-1}$) in the regression model that treats R_{mL} as the dependent variable (Fig. 5).

There is considerably less overlap between the WES (Chave et al. 2009) and the functional traits in the ACGCA model, with only wood density (ρ) being explicitly included in both. However, the proportion of xylem conducting area (γ_X) is an important wood trait in ACGCA, and it can be derived from traits in the WES, including mean conduit diameter and conduit density (i.e., number of conduits per cross-sectional area), given assumptions about conduit shape (e.g., circular cross section). In the WES, conduit density is often found to be negatively correlated with ρ (Chave et al. 2009). This is in agreement with our TTS; the bivariate correlation between ρ and γ_X and the associated partial regression coefficients were both negative and significant. Our study also suggests that the WES could be expanded upon by considering other wood traits (e.g., R_{mS} , S_C , SW_{max}) that emerged here as important predictors of traits included in the WES (γ_X and ρ ; Fig. 5) and/or of tree growth (Fig. 4).

The general agreement between patterns contained in our TTS and analogous aspects of common, empirical trait spectra (LES and WES) suggests that quantifying the TTS provides another approach to understanding trade-offs among functional traits. The ACGCA model directly incorporates mass conservation (via carbon allocation, utilization, and storage mechanisms) and engineering trade-offs (via structural and allometric relationships; Scheiter et al. 2013). The TTS produced by the ACGCA model contained trait trade-offs similar to those seen in the LES and WES, at least in direction (positive vs. negative), suggesting that mass conservation and

engineering trade-offs likely govern much of the variation in these empirical spectra. It is notable that prominent empirical trait relationships were contained in the TTS, despite the fact that the ACGCA model, as implemented here, did not include important factors such as water limitations, nutrient availability, disturbances, or biotic interactions that act on actual trees. If such factors are included in theoretical (modeling) analyses of functional trait spectra, they could possibly generate a more refined description of how specific physiological and environmental processes influence the functional trait space.

Caveats of our TTS approach and future directions

One concern that could arise from our approach of fitting a fairly complex IBM (the ACGCA model) to the aggregated FIA data is non-identifiability of some of the parameters (traits). There are two reasons, however, why this potential issue is of little concern in this study. First, the approach clearly eliminates combinations of parameter (trait) values that are inconsistent with the FIA data (e.g., Fig. 1a, b, d, e). For instance, the ACGCA model is capable of simulating a tree that grows over 100 m in a few years, given certain (unrealistic) combinations of parameter values. While the value of each parameter (trait) may be observable in nature, the particular combination of values is unlikely to exist in nature, and such combinations are subsequently eliminated by fitting the model to the FIA data. Second, the ACGCA model incorporates engineering and mass-balance trade-offs in the form of equations linking physiological, allocation, and allometric constraints motivated by years of research on these processes (Ogle and Pacala 2009). While it is possible that multiple combinations of trait value will lead to similar growth dynamics, the parameter values will “travel along” trait manifolds contained within the ACGCA model. Thus, fitting the ACGCA model to the FIA enables the exploration of these manifolds and associated inferences about engineering and/or mass-balance trade-offs predicted by the theoretical (i.e., semi-mechanistic) model of tree growth, as constrained by data on real tree growth (via the FIA database and literature-based priors). Fitting the model to additional types of data—such as mortality (live/dead

status) and independent measures of biomass—would likely help to solve potential identifiability issues given that our sensitivity analysis found different sets of traits to be predictive of growth vs. labile carbon status.

Related to the above identifiability issue, our approach to quantifying the TTS is agnostic to site conditions or species identity. Binning the FIA data by both site and species would have produced an insufficient number of data points to develop representative four-dimensional histograms (*Hist*) of observed heights, radii, and associated growth rates for each bin. However, we would expect that binning by species, for abundant species, may have produced trait spaces that differed among species, with each being contained in the overall TTS described here for a “generic” North American tree in a healthy, growing state.

Moreover, the TTS presented here represents a multidimensional hypervolume of traits that does not explicitly account for other potentially important environmental factors (e.g., moisture, disturbances) or biotic interactions (e.g., competition). For instance, this study focused on light as the sole environmental driver; filtering the TTS by limiting the range of values associated with four traits (f_L , SLA , R_{mL} , and R_{40} ; see Table 1) and light level (PAR_{max}) revealed a potential trade-off (correlation) between root maintenance respiration (R_{mR}) and radiation-use efficiency (ϵ ; see Fig. 7; Appendix S1: Fig. S3). Filtering by light represents a particular environmental constraint, while filtering by the other four traits represents potential environmental or biotic selection pressures. If other drivers and filtering processes had been explicitly accounted for in our analyses, the resulting trait space associated with different scenarios would likely have been refined relative to the TTS described herein. This refinement or filtering of the TTS to reflect additional constraints on tree growth may have resulted in stronger bivariate relationships among traits, representing more pronounced trade-offs under specific conditions, or may have identified a different subset of coordinated traits.

Other trait spaces could be constructed with different process-based models of tree or plant function, or by including species-specific traits and fitting to data on individual trees or species. The parameters in such models can generally be interpreted as plant traits, and for comparison against field-based empirical spectra, at least a

subset of parameters should overlap with traits in such empirical spectra. We could further refine the TTS emergent from the ACGCA model by including additional environmental limitations. For instance, the modular structure of the ACGCA model could accommodate a more mechanistic model of carbon acquisition, but incorporating, for example, the Farquhar et al. (1980) model of photosynthesis and a stomatal conductance model (Ball et al. 1987, Leuning 1995, Ogle and Reynolds 2002, Medlyn et al. 2011). Incorporation of a more mechanistic photosynthesis model, along with a water transport model, could allow for the possible incorporation of a full representation of the soil–plant atmosphere continuum (Sperry et al. 1998, Tuzet et al. 2003), and thus, evaluation of the effects of water availability on the TTS. The type of model-based analysis conducted herein could provide unique opportunities to investigate how specific processes—such as those related to physiology, mass conservation, and engineering constraints—interact with each other to govern functional trait distributions and trade-offs.

CONCLUSIONS

In summary, in the absence of fitting the ACGCA model to the FIA data, randomly chosen combinations of parameters can result in trees that grow unrealistically fast, tall, or wide, trees that do not grow, or trees that immediately die, even under high-light conditions (Fig. 1c, f). For example, combining high values of *SLA* and ϵ with low values of respiration, construction costs, and senescence rates will lead to a tree that unrealistically reaches its maximum height within one annual time step. Thus, the trade-offs that emerge by fitting the ACGCA model to the FIA and Tree-Traits data represent a combination of the mass-balance and engineering mechanisms that are built into the model, combined with empirical relationships contained in the FIA data.

Though strong bivariate patterns among traits did not directly emerge from the TTS described by the posterior distribution of parameters (θ) in the ACGCA model, complex multidimensional relationships are contained in this trait space, for at least a subset of traits. Thus, the TTS implies that realistic tree growth can only be predicted if the multivariate structure of a subset of traits

(subset of θ) is maintained; if individual traits within with the TTS are randomly combined, this leads to immediate tree death in the vast majority of simulations. The TTS also suggested a number of root traits and other less commonly quantified traits may be important for understanding trait spectra, whole-plant performance (e.g., growth), and life-history trade-offs, and such traits should be considered in future observational and experimental studies. Finally, the directions (positive or negative) of the trait–trait relationships in the TTS generally agreed with existing empirical spectra (e.g., LES and WES), pointing to the validity of using mechanistic models to explore the TTS, while also suggesting mechanisms giving rise to the observed variation in empirical trait spectra.

ACKNOWLEDGMENTS

This work was supported by an NSF grant to Ogle and Barber (DBI no. 0850361 and no. 1133366). We thank Jessica Guo, Drew Peltier, Edmund Ryan, and Heather Kropp for valuable input on the manuscript. We thank Fell's remaining committee members for their support and feedback, including Janet Franklin, Thomas Day, and Kevin Hultine. Fell conducted all simulations and most data analyses and wrote the manuscript; Barber assisted with the MH algorithm, simulations, and data analysis and contributed to manuscript writing; Lichstein provided the FIA data and contributed to manuscript writing; Ogle conceived the study, supervised simulations and analyses, and co-wrote the manuscript.

LITERATURE CITED

- Adler, P. B., R. Salguero-Gómez, A. Compagnoni, J. S. Hsu, J. Ray-Mukherjee, C. Mbeau-Ache, and M. Franco. 2014. Functional traits explain variation in plant life *history* strategies. *Proceedings of the National Academy of Sciences* 111:740–745.
- Atkin, O. K., et al. 2015. Global variability in leaf respiration in relation to climate, plant functional types and leaf traits. *New Phytologist* 206:614–636.
- Ball, J., I. E. Woodrow, and J. Berry. 1987. A model predicting stomatal conductance and its contribution to the control of photosynthesis under different environmental conditions. Pages 221–224 *in* *Progress in Photosynthesis Research*. Springer, Dordrecht, The Netherlands.
- Baraloto, C., C. E. T. Paine, L. Poorter, J. Beauchene, D. Bonal, A. M. Domenach, B. Hérault, S. Patiño, J. C. Roggy, and J. Chave. 2010. Decoupled leaf and stem economics in rain forest trees. *Ecology Letters* 13:1338–1347.

- Bechtold, W. A., and P. L. Patterson. 2005. The Enhanced Forest Inventory and Analysis Program—national sampling design and estimation procedures. USDA General Technical Report SRS-80:85. U.S. Department of Agriculture, Asheville, North Carolina, USA.
- Bugmann, H. 2001. A review of forest gap models. *Climatic Change* 51:259–305.
- Cavender-Bares, J., K. Kitajima, and F. A. Bazzaz. 2004. Multiple trait associations in relation to habitat differentiation among 17 Floridian oak species. *Ecological Monographs* 74:635–662.
- Chave, J., D. Coomes, S. Jansen, S. L. Lewis, N. G. Swenson, and A. E. Zanne. 2009. Towards a worldwide wood economics spectrum. *Ecology Letters* 12:351–366.
- Chave, J., et al. 2008. Assessing evidence for a pervasive alteration in tropical tree communities. *PLoS Biology* 6:455–462.
- Damour, G., T. Simonneau, H. Cochard, and L. Urban. 2010. An overview of models of stomatal conductance at the leaf level. *Plant, Cell and Environment* 33:1419–1438.
- Díaz, S., et al. 2004. The plant traits that drive ecosystems: evidence from three continents. *Journal of Vegetation Science* 15:295–304.
- Díaz, S., et al. 2016. The global spectrum of plant form and function. *Nature* 529:167–171.
- Domec, J.-C., B. Lachenbruch, F. C. Meinzer, D. R. Woodruff, J. M. Warren, and K. A. McCulloh. 2008. Maximum height in a conifer is associated with conflicting requirements for xylem design. *Proceedings of the National Academy of Sciences* 105:12069–12074.
- Evans, M. R. 2012. Modelling ecological systems in a changing world. *Philosophical Transactions of the Royal Society B* 367:181–190.
- Evans, J. R., and H. Poorter. 2001. Photosynthetic acclimation of plants to growth irradiance: the relative importance of specific leaf area and nitrogen partitioning in maximizing carbon gain. *Plant, Cell and Environment* 24:755–767.
- Falster, D. S., Å. Brännström, U. Dieckmann, and M. Westoby. 2011. Influence of four major plant traits on average height, leaf-area cover, net primary productivity, and biomass density in single-species forests: a theoretical investigation. *Journal of Ecology* 99:148–164.
- Falster, D. S., Å. Brännström, M. Westoby, and U. Dieckmann. 2017. Multitrait successional forest dynamics enable diverse competitive coexistence. *Proceedings of the National Academy of Sciences* 114:201610206.
- Farquhar, G. D., S. Caemmerer, and J. A. Berry. 1980. A biochemical model of photosynthetic CO₂ assimilation in leaves of C3 species. *Planta* 149:78–90.
- Fisher, R. A., et al. 2015. Taking off the training wheels: the properties of a dynamic vegetation model without climate envelopes, CLM4.5(ED). *Geoscientific Model Development* 8:3593–3619.
- Fyllas, N. M., et al. 2014. Analysing Amazonian forest productivity using a new individual and trait-based model (TFS v. 1). *Geoscientific Model Development* 7:1251–1269.
- Gelman, A., J. B. Carlin, H. S. Stern, D. B. Dunson, A. Vehtari, and D. B. Rubin. 2014. *Bayesian data analysis*. Third edition. CRC Press, Boca Raton, Florida, USA.
- Gelman, A., G. Roberts, and W. Gilks. 1996. Efficient metropolis jumping rules. *Bayesian Statistics* 5:599–607.
- Gemoets, D., J. Barber, and K. Ogle. 2013. Reversible jump MCMC for inference in a deterministic individual-based model of tree growth for studying forest dynamics. *Environmetrics* 24:433–448.
- Kattge, J., K. Ogle, G. Bönisch, S. Díaz, S. Lavorel, J. Madin, K. Nadrowski, S. Nöllert, K. Sartor, and C. Wirth. 2011. A generic structure for plant trait databases. *Methods in Ecology and Evolution* 2:202–213.
- Kutner, M. H., C. J. Nachtsheim, J. Neter, and W. Li. 2005. *Applied linear statistical models*. Fifth edition. McGraw-Hill Irwin, Boston, Massachusetts, USA.
- Lavorel, S., S. Díaz, J. H. C. Cornelissen, E. Garnier, S. P. Harrison, S. Mcintyre, J. G. Pausas, N. P. Catherine, and R. Carlos. 2007. Plant functional types: Are we getting any closer to the holy grail? Pages 149–164 in J. G. Canadell, D. E. Pataki, and L. F. Pitelka, editors. *Terrestrial ecosystems in a changing world*. First edition. Springer, New York, New York, USA.
- Lavorel, S., and E. Garnier. 2002. Predicting changes in community composition and ecosystem functioning from plant traits. *Functional Ecology* 16:545–556.
- Leuning, R. 1995. A critical appraisal of a combined stomatal-photosynthesis model for C3 plants. *Plant Cell and Environment* 18:339–355.
- Lloyd, J., K. Bloomfield, T. F. Domingues, and G. D. Farquhar. 2013. Photosynthetically relevant foliar traits correlating better on a mass vs an area basis: Of ecophysiological relevance or just a case of mathematical imperatives and statistical quicksand? *New Phytologist* 199:311–321.
- Lunn, D., D. Spiegelhalter, A. Thomas, and N. Best. 2009. The BUGS project: evolution, critique and future directions. *Statistics in Medicine* 28:3049–3067.
- Martin, T. A., and E. J. Jokela. 2004. Developmental patterns and nutrition impact radiation use efficiency components in southern pine stands. *Ecological Applications* 14:1839–1854.
- Medlyn, B. E., R. A. Duursma, D. Eamus, D. S. Ellsworth, I. C. Prentice, C. V. M. Barton, K. Y. Crous, P. De Angelis, M. Freeman, and L. Wingate. 2011.

- Reconciling the optimal and empirical approaches to modelling stomatal conductance. *Global Change Biology* 17:2134–2144.
- Ogle, K., J. Barber, and K. Sartor. 2013. Feedback and modularization in a Bayesian meta-analysis of tree traits affecting forest dynamics. *Bayesian Analysis* 8:133–168.
- Ogle, K., and S. W. Pacala. 2009. A modeling framework for inferring tree growth and allocation from physiological, morphological and allometric traits. *Tree Physiology* 29:587–605.
- Ogle, K., S. Pathikonda, K. Sartor, J. W. Lichstein, J. L. D. Osnas, and S. W. Pacala. 2014. A model-based meta-analysis for estimating species-specific wood density and identifying potential sources of variation. *Journal of Ecology* 102:194–208.
- Ogle, K., and J. F. Reynolds. 2002. Desert dogma revisited: coupling of stomatal conductance and photosynthesis in the desert shrub, *Larrea tridentata*. *Plant, Cell and Environment* 25:909–921.
- Osnas, J. L. D., J. W. Lichstein, P. B. Reich, and S. W. Pacala. 2013. Global leaf trait relationships: mass, area, and the leaf economics spectrum. *Science* 340:1–4.
- Plummer, M. 2003. JAGS: a program for analysis of Bayesian graphical models using Gibbs sampling. *Proceedings of the 3rd International Workshop on Distributed Statistical Computing*: 20–22.
- Plummer, M., N. Best, K. Cowles, and K. Vines. 2006. Convergence diagnosis and output analysis for MCMC. *R News* 6:7–11.
- R Core Team. 2015. R: a language and environment for statistical computing. R Foundation for Statistical Computing, Vienna, Austria.
- Reich, P. B. 2014. The world-wide “fast-slow” plant economics spectrum: a traits manifesto. *Journal of Ecology* 102:275–301.
- Reich, P. B., D. S. Ellsworth, M. B. Walters, J. M. Vose, C. Gresham, J. C. Volin, and W. D. Bowman. 1999. Generality of leaf trait relationships: a test across six biomes. *Ecology* 80:1955–1969.
- Reich, P. B., M. B. Walters, and D. S. Ellsworth. 1997. From tropics to tundra: global convergence in plant functioning. *Proceedings of the National Academy of Sciences* 94:13730–13734.
- Sakschewski, B., W. von Bloh, A. Boit, A. Rammig, J. Kattge, L. Poorter, J. Peñuelas, and K. Thonicke. 2015. Leaf and stem economics spectra drive diversity of functional plant traits in a dynamic global vegetation model. *Global Change Biology* 21:2711–2725.
- Scheiter, S., L. Langan, and S. I. Higgins. 2013. Next-generation dynamic global vegetation models: learning from community ecology. *New Phytologist* 198:957–969.
- Shipley, B., M. J. Lechowicz, I. Wright, and P. B. Reich. 2006. Fundamental trade-offs generating the worldwide leaf economics spectrum. *Ecology* 87: 535–541.
- Sinclair, T. R., and T. Horie. 1989. Leaf nitrogen, photosynthesis, and crop radiation use efficiency: a review. *Crop Science* 29:90.
- Sperry, J. S., F. R. Adler, G. S. Campbell, and J. P. Comstock. 1998. Limitation of plant water use by rhizosphere and xylem conductance: results from a model. *Plant, Cell and Environment* 21:347–359.
- Stahl, U., J. Kattge, B. Reu, W. Voigt, and K. Ogle. 2013. Whole-plant trait spectra of North American woody plant species reflect fundamental ecological strategies. *Ecosphere* 4:128.
- Suzuki, E. 1999. Diversity in specific gravity and water content of wood among Bornean tropical rainforest trees. *Ecological Research* 14:211–224.
- Tuzet, A., A. Perrier, and R. Leuning. 2003. A coupled model of stomatal conductance, photosynthesis and transpiration. *Plant, Cell and Environment* 26:1097–1116.
- Van Bodegom, P. M., J. C. Douma, and L. M. Verheijen. 2014. A fully traits-based approach to modeling global vegetation distribution. *Proceedings of the National Academy of Sciences* 111:13733–13738.
- Wang, A. Y. P., P. G. Jarvis, and C. M. Taylor. 1991. PAR absorption and its relation to above-ground dry matter production of Sitka spruce. *Journal of Applied Ecology* 28:547–560.
- Webb, C. T., J. A. Hoeting, G. M. Ames, M. I. Pyne, and N. LeRoy Poff. 2010. A structured and dynamic framework to advance traits-based theory and prediction in ecology. *Ecology Letters* 13: 267–283.
- Weiher, E., A. van der Werf, K. Thompson, M. Roderick, E. Garnier, and O. Eriksson. 1999. Challenging Theophrastus: a common core list of plant traits for functional ecology. *Journal of Vegetation Science* 10:609–620.
- Wright, I. J., et al. 2004. The worldwide leaf economics spectrum. *Nature* 428:821–827.

SUPPORTING INFORMATION

Additional Supporting Information may be found online at: <http://onlinelibrary.wiley.com/doi/10.1002/ecs2.2060/full>